Faculty

Engineering

SINGLE AND BINARY GAS TRANSPORT OF H_2, CO AND CO_2 THROUGH A NaA-CENTRIFUGALLY CASTED ALUMINA COMPOSITE MEMBRANE

Willem Frederik Breedt Louw

B.Eng. (North-West University, Potchefstroom Campus)

This dissertation is presented in partial fulfilment of the requirements for the degree Masters of Engineering in the School of Chemical and Minerals Engineering at North-West University, Potchefstroom Campus.

Supervisor:	Prof HWJP Neomagus
Co-supervisor	Prof RC Everson

ACKNOWLEDGEMENTS

I would like to use this opportunity to thank all of the people that made a contribution to this project:

Prof. Hein Neomagus for his guidance in this particular project. He showed extensive patience in explaining certain concepts and gave me great insight into the methodology of research. The occasional beer in Castilions also proved to be of cardinal importance in planning the project as it evolved.

Mr. Jan Kroeze and all the technical staff at the School of Chemical and Minerals Engineering.

DECLARATION

Hereby I, Willem Frederik Breedt Louw, declare that the dissertation with the title SINGLE AND BINARY GAS TRANSPORT OF H_2, CO AND CO_2 THROUGH A NaA- CENTRIFUGALLY CASTED ALUMINA COMPOSITE MEMBRANE in partial fulfilment of the requirements for the M. Eng. degree, is my work and has not been submitted at any other university either in whole or in part.

Signed at Potchefstroom.

_____ _____

Willie Louw Date

ABSTRACT

NaA (or Linde Type A: $|Na^{+}_{12}\ (H_2O)_{27}|_8\ [Al_{12}Si_{12}\ O_{48}]_8$ –LTA) membranes were prepared on centrifugally casted alumina supports and tested for its permeation and separation properties using single gasses and binary mixtures of H_2, CO, CO_2. 2 membranes were prepared: one with a double and one with a triple NaA layer. From single permeation experiments it was concluded that the triple coated NaA membrane gave better selectivities than the double coating one, but the selectivities were still in the range of Knudsen selectivities. Significant permeation of SF_6 was also observed, which indicated that intracrystalline diffusion could not be neglected.

From the single gas permeation experiments, using the triple coated membrane, the important transport mechanisms were determined and it was shown that the resistance in the support can be as high as 60%, depending on the applied pressure difference and temperature. The resistance in the support itself is predominant Knudsen diffusion, due to the relative small average pore radius of the support.

The permeability of the NaA layer was higher than NaA membranes presented in the open literature, which were tested under similar conditions, which could also be attributed to the occurrence of intracrystalline diffusion.

The selectivity of the membranes in binary mixtures of CO_2/H_2, CO/H_2 and CO_2/CO were very close to unity, showing that the used triple coated NaA membrane was not suited for the separation of any of the studied gases.

A reason for the bad performance of the membrane could be the relative short time used for the growth of the NaA crystals. Microscopic inspection showed that the crystal growth was not complete, and together with the hydrophilic character of the NaA zeolite this was probably the main reason for the occurrence of intracrystalline diffusion. A longer synthesis time was therefore also recommended.

TABLE OF CONTENTS

LIST OF FIGURES

LIST OF TABLES

NOMENCLATURE

Symbol	Description	Units
A	Membrane surface area	m^2
C	Concentration	mol/m^3
ΔC	Concentration gradient	mol/m^3
D	Transport diffusivity	m^2/s
d_p	Pore diameter	m
E_a	Activation energy	J/mol
g	Geometric factor	-
H	Height counts	-
J	Flux	$mol/m^2.s$
K_N	Knudsen number	-
Kn	Knudsen diffusion ratio	-
l	Membrane length	m
M_w	Molecular weight	kg/mol
M2	Double coated membrane	-
M3	Triple coated membrane	-
P	Pressure	Pa
$\overline{P}$	Average pressure between shell and tube side	Pa
ΔP	Trans membrane pressure	Pa
q_{sat}	Saturation concentration in zeolite	mol/kg
R	Universal gas constant	J/mol.K
r_p	Zeolite pore radius	m
r_s	Shell side radius	m
r_t	Tube side radius	m
T	Temperature	K
Δx	Membrane thickness	m
y	Molar fraction	-

Greek	Description	Units
α	Membrane selectivity	-
Π	Permeability	$mol/m^2.s.Pa$
η	Viscosity	Pa.s
ε	Porosity	-
ϕ_m	Molar flow rate	mol/s
ϕ_v	Volumetric flow rate	m^3/s
θ	Occupancy	-
ρ	Zeolite density	kg/m^3
τ	Tortuosity	-

Subscripts	Description
F	Feed
i,j	Different species
mem	Membrane
perm	Permeate
ret	Retentate
sup	Support
Superscripts	**Description**
Kn	Knudsen diffusion
S	Surface diffusion
vis	Viscous flow

Acronym	Description
BPR	Back pressure regulator
CGM	Concentration gradient method
ED	Electrodialysis
GS	Gas separation
IEA	International Energy Agency
MC	Membrane contactors
MD	Membrane distillation
ME	Membrane electrolysis
MF	Microfiltration
MFC	Mass flow controller
NF	Nanofiltration
NWU	North-West University
PDM	Pressure drop method
PV	Pervaporation
UF	Ultrafiltration
RO	Reverse osmosis
SFM	Soap flow meter
VP	Vapour permeation

CHAPTER 1: INTRODUCTION

1.1 BACKGROUND

Sustainable development has been an important part of public policy debate the last few years. This very broad concept covers human activities that have an impact on economic development, environmental issues and social well-being. A generally accepted definition is; *development that meets the needs of the present generation without undermining the capacity of the future generations to meet their needs* [1]. Although this covers a very broad scale of activities, the future supply of energy should certainly form a central part of all developments concerned with it.

According to the International Energy Agency's (IEA) World Energy Outlook [2], global energy demands will increase with 1.7% per year from 2002 to 2030. In order to sustain this relentless increase (roughly two-third of the current consumption), fossil fuels will have to account for more than 90% of these needs and other predictions include [2]:

- The use of oil will increase from 77 to 120 million barrels per day in 2030.
- New power stations will account for over 60% of the increase in fuel demand over the next 30 years.
- Coal consumption will expand slower than other fuels.
- Nuclear power will decline due to the lack of new reactors.
- Non-hydro renewable energy sources (especially wind power and biomass) will also increase in importance.

Although these predictions sound pessimistic, the world's energy resources are adequate to meet the projected energy growth for the coming decades. The prediction that coal consumption is expected to slow is however debatable, with crude oil reaching record selling prices in excess of 75 $/barrel in 2006, especially since Sasols'

well established CTL technology is becoming more popular in coal rich areas. For similar reasons the decline in nuclear reactors can also be questioned. Especially since Iran is planning on improving its nuclear program – what message is sent out to less fortunate (energy deprived) countries concerned about their future energy needs. Never the less areas with large hydrocarbon resources, like the Middle East and Soviet Union, will be able to meet much of the oil and gas demand. Natural gas production will increase in most regions except for Europe. Coal production will be concentrated in South Africa, Australia, China, India, Indonesia, North America, and Latin America where mining, processing and transport costs are the lowest. Other sources of energy will include non-conventional sources of oil, fuel cells based on steam reforming and advanced and/or new technologies.

The IEA lists two very important energy diversification possibilities for the future [2]:

- Importance of coal.
- The move towards a hydrogen economy.

Although these are seen as individual steps to a unified global challenge for energy security, they seem to have a unique *relationship* in countries that rely heavily on or can supply ample quantities of coal. According to another study by the IEA [3] the move towards a hydrogen economy is predicted to grow sharply in the next 50 to 100 years. In essence, this hydrogen economy aims on the direct use of H_2 as fuel for two new fundamentally different applications such as the production of electricity and for transportation. This comes as a result of global warming, low oil/gas reserves and the need to adopt an energy security policy for the future.

But where does this *relationship* lie? It can be found once the answer to the next question is obtained – where will the hydrogen come from?

Figure 1-1 shows the possible alternatives for hydrogen production and also lists coal as a possible source. H_2 currently produced from the gasification of coal is essentially used as an intermediate for the production of chemicals such as methanol,

ammonia/urea, methane or Fischer-Tropsch products. However, techno-economic studies done by the IEA [3] show that there are prospects for the production of H_2 from coal, but stresses the need for the development of new technologies.

By using H_2 instead of fossil fuels as a source of energy, the only by-product formed is water. However, the generation of H_2 from coal and other fossil fuels is accompanied by the production of CO_2, CH_4 and various other polluting gasses. While considering new ways for the production and separation of H_2, it becomes essential to develop technologies for the removal of these pollutants. The use of H_2 in the medium term seems like an attractive transitional energy strategy while we await the use of H_2 as a future energy carrier.

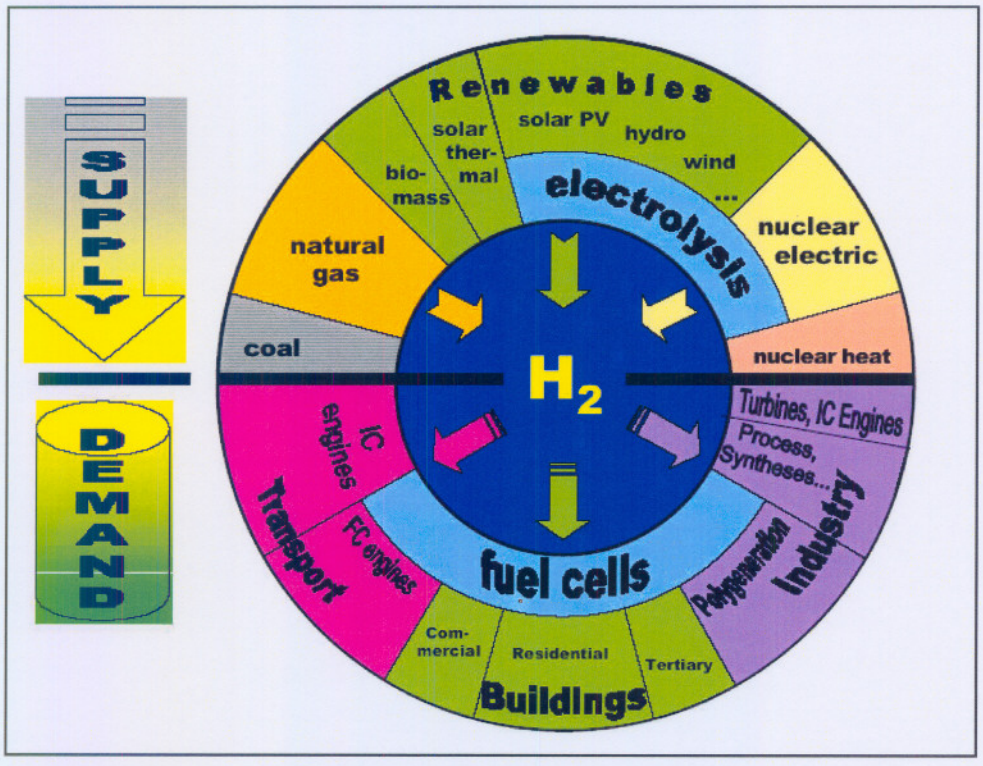

Figure 1-1: Hydrogen production alternatives [Taken from 4]

(Note that the sizes of sectors have no connection with current or expected markets)

Since coal is going to remain an integral proportion of H_2 sources in the foreseeable future the separation of gas mixtures containing H_2, CO_2, CO and CH_4 will continue to have a wide application in industry, especially in H_2/CO_2 separation. Existing technologies for H_2/CO_2 separation include absorption processes (chemical, physical or hybrid), adsorption processes and cryogenic separation. Most of these CO_2 capture technologies operate at low temperature, requiring the synthesis gas produced in the gasifier to be cooled, just to be heated once the CO_2 is removed. Membrane technology provides a possible solution to this problem and is capable of substantial cost reduction in separation processes due to its low energy consumption and wide range of operating conditions *e.g.* temperature, pressure and chemical environment.

Zeolite based membranes have generated much interest over the past decade, primarily for its molecular sieving properties. According to Funke *et al.* [5] zeolites are "*microporous, crystalline materials with narrow pore size distribution on a molecular scale and high thermal, chemical and mechanical stability*". Based on these characteristics, zeolite membranes are capable highly selective separation and low energy consumption; process conditions ideal for sustainable development in the 21st century.

1.2 MOTIVATION AND OBJECTIVES

The North West University (NWU) together with the University Twente (The Netherlands) developed a unique production process of ceramic membranes. The novelty of the composite membranes is in the manufacture of the support, which is an essential step in the production of thin, high permeability, zeolite based membranes. The supports are made via centrifugal casting, in which the green body is rotated against 15000 – 20000 rpm, in order to get a support with a very smooth surface after sintering. This smooth surface has improved properties for zeolite growth, compared to conventional slip casting based supports (6). In this way, silicalite and NaA membranes have been prepared, and tested for pervaporation applications, with separation factors of up to 25 000 for NaA in the dehydration of water-ethanol mixtures (6).

The aim of this investigation is to use the existing technology of membrane preparation and extend the field of application to gas separation. In the first instance single gas permeation experiments will be carried out in order to characterise and determine transport phenomena of H_2, CO_2 and CO using a NaA zeolite membrane. Secondly, binary permeation experiments will be conducted to verify the application of a NaA membrane in gas separation environment. This, in order to assist with the development of separation processes for the removal/purification of one of these components in gas streams typical to the coal processing industry.

The specific objectives of this study are:

- Design/acquire, construct and commission the individual components necessary to carry out the experiments. This includes the construction of a membrane module.
- Study single gas permeation of H_2, CO, CO_2 as a function of the process parameters temperature, pressure and pressure difference
- From the single gas permeation experiments: to identify and quantify the importance of different transport mechanisms across the composite membrane.
- To investigate the possibility of separation of binary mixtures of H_2, CO and CO_2

1.3 SCOPE OF INVESTIGATION

In Chapter 1, the need for sustainable development is discussed, with particular reference to sustainable energy resources and the medium and long term goals to achieve this. Here the role of membrane technology is introduced as a possible solution to assist in meeting the medium term goals.

In Chapter 2 all the relevant information to this study are given regarding gas separation and zeolite membranes. The chapter begins with an overview of membrane terminology and classifications, followed by a discussion regarding the use of membranes for gas separation applications in industry. Chapter 2 is also used to give background information on zeolite membranes, their structures and other relating issues. This is followed by an overview of the literature on zeolite membranes used for gas separation application, with particular reference to articles containing information about H_2, CO and CO_2 permeation. Finally, the relevant literature with regard to transport mechanisms across zeolite membranes is given.

Chapter 3 deals with the experimental issues of the study. All the relevant equipment is discussed as well as the procedures used during support casting, membrane synthesis and experimental procedures.

Chapter 4 contains all the experimental results and discussion thereof while the conclusions and recommendations are given in chapter 5.

CHAPTER 2: LITERATURE REVIEW

2.1 MEMBRANE PROCESSES

2.1.1 BRIEF OVERVIEW OF MEMBRANES

In its earlier stages of development membrane science focussed mostly on naturally occurring membranes [7]. This later evolved into a scientific discipline and is one of the promising steps in making sustainable development a reality. Today membrane applications range from concentration to purification and fractionation of different systems.

According to *Mulder* [8], a membrane may be defined as "*a permselective barrier between two homogeneous phases.*" *Meares* [9] describes a membrane system as two uniform, homogeneous and three-dimensional fluid phases "*between which matter and energy may be exchanged at rates governed by the properties of a third phase, or group of phases, which separates them.*" A third definition is given by *Hsieh* [7], who states that a membrane can be a semi-permeable active or passive barrier that permits preferential passage of one or more species under a certain driving force.

From the above-mentioned definitions, it is clear that a certain driving force must be present to bring about the required separation. These forces can exist in the form of pressure, concentration or electrochemical potential difference across the membrane. Depending on these driving forces and the physical size of the species involved, membrane processes are classified according to first and second-generation membrane processes [8]. First generation processes include microfiltration (MF), ultrafiltration (UF), nanofiltration (NF), reverse osmosis (RO), dialysis, electrodialysis (ED), and membrane electrolysis (ME) while second generation membrane processes are gas separation (GS), vapour permeation (VP), pervaporation (PV), membrane

distillation (MD), membrane contactors (MC) and carrier mediated processes.

During membrane processes the primary species that are rejected are referred to as the retentate while those species passing along the membrane are termed permeate. The selectivity of a membrane for gas separation of species i and j is normally quantified by the separation factor α, defined as:

$$\alpha = \frac{y_{i,perm} / y_{j,perm}}{y_{i,ret} / y_{j,ret}} \tag{2.1}$$

in which, conventionally, *i* is the fastest permeating specie. This equation can however only give a solid characteristic of the membrane itself if the membrane module is operated at differential conditions or at low selectivities. There are primarily two modes of operation for membrane processes, classified according to the direction of the feed stream relative to the orientation of the membrane surface: dead-end filtration and crossflow filtration *(Figure 2-1)*.

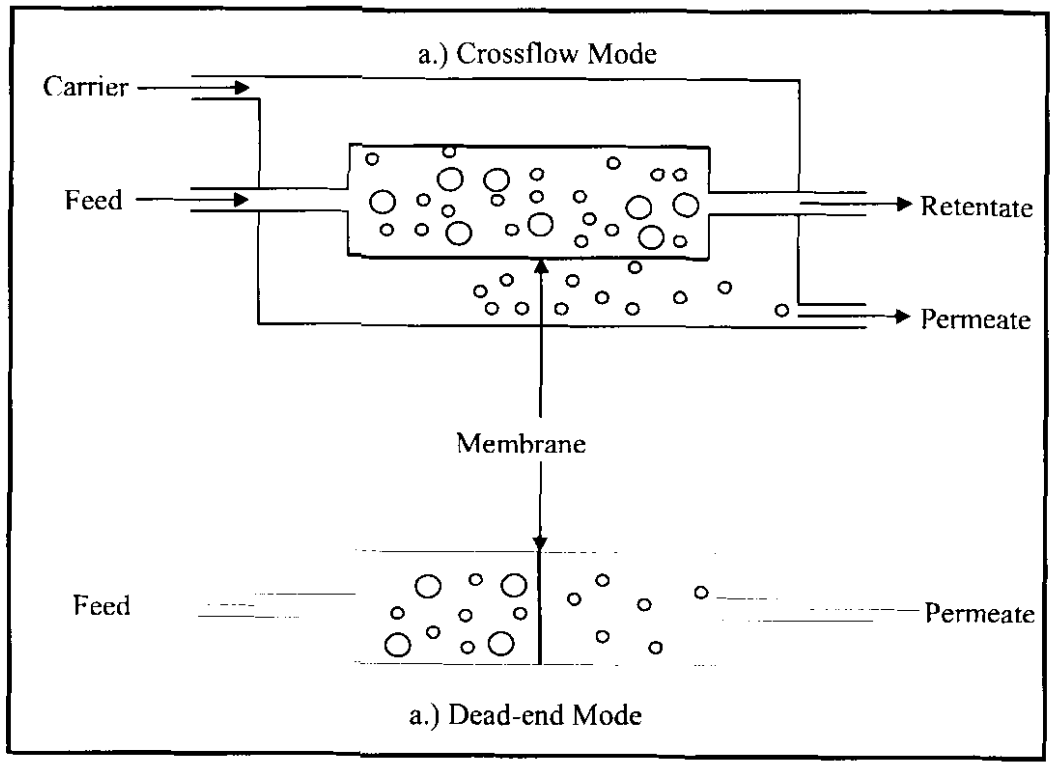

Figure 2-1: Modes of operation for a membrane process: a.) Crossflow filtration mode and b.) Dead-end filtration mode [7]

A number of other classifications also exist where classification is based on the membrane structure. Here the terms dense, porous, symmetric or asymmetric are used to describe the membrane. A final classification is to order the membranes in terms of the materials they are composed of, i.e. biological and synthetic membranes. Synthetic membranes can further be divided into organic and inorganic membranes where inorganic membranes have the advantage of thermal, chemical and mechanical stability.

2.2 MEMBRANE TECHNOLOGY

2.2.1 INTRODUCTION

Membrane technology has become a competitive separation technique over the past decades, mainly due to the use in water separation and purification applications. Other industrial applications range from nitrogen production, separating hydrocarbons from air and nitrogen and hydrogen recovery systems. Also, membrane technology is used for power generation, tissue repair, protective garments, pharmaceutical production, food and beverage processing fuels and electronics. As discussed earlier, the primary forces for the introduction of membrane technology are the consumer demand for higher quality products, increased regulatory pressures, deteriorating natural resources, and the need for environmental and economic sustainability. Membranes capable of selectively separating various gasses or gas mixtures will certainly find a niche in the majority of these markets.

2.2.2 MEMBRANES FOR GAS SEPARATION

Generally, gas separating membranes are divided into three categories [10], where the structure of the membrane determines the mechanism of separation. For the first mechanism, transport is governed by Knudson diffusion. In this, regime pore sizes typically range between 2 and 50 nm and separation is based on differences in

molecular weight. For pore sizes larger than 50 nm convective transport also plays a role, and selectivities normally decrease in this case.

If pore sizes become smaller than 2 nm, molecules can be excluded from pores based on their size. This is referred to as molecular sieving. In such small pores, surface diffusion also becomes important which means that separation can also be based on the affinity of a molecule toward the pore wall.

A third type of membrane comprises the dense membranes. These membranes do not have pores and transport occurs by dissolution of components in the dense matrix followed by diffusion through the matrix. Component solubility and mobility in these membranes thus determines the degree of separation.

Industrial applications of membranes in gas separation are found in the production of nitrogen from air [10]. Polymer membranes are currently the only membranes that are used at an industrial scale for H_2 and CO_2 separation from coal synthesis gas, although some interesting developments have been reported [3]. Table 2-1 summarises the findings of the IEA [3] with respect to membrane technologies used for the separation of H_2 and CO_2 in the coal industry.

Table 2-1: Comparative table for H_2/CO_2 separation in membranes (Adapted from [3])

Summary of gas separation membranes used in H_2/CO_2 separation			
Type	**Advantages**	**Drawbacks**	**Prospects**
Dense ceramic	-Hydrogen selectivity 100% -No pore clogging -Inexpensive materials	-Low permeation rates -Unstable in presence of high CO_2 concentrations	-H_2 target flux: 8.10^{-3} $m^3/m^2.s$ for a differential pressure of 2.8 MPa at temperatures below 600°C
Porous ceramic	-High permeation rates -H_2 flux directly proportional to pressure differential -Cheap material	-Not H_2 selective -Difficult to produce defect free membrane -Not sufficiently tested under real operating conditions	-H_2 target flux: 8.10^{-2} $m^3/m^2.s$ for a differential pressure of 3 MPa -Development of defect-free microporous membranes -Development of zeolite based molecular sieve membranes
Metallic (Pd based)	-Hydrogen selectivity 100% -Not affected by CO_2 in gas streams	-Cost of Pd is prohibitive -Problems associated during thermal recycling	-Development of thin Pd membranes to reduce cost -Development of Pd alloys thermally, chemically and mechanically more resistant than pure Pd membranes
Polymer	-Only membrane developed at industrial scale for gas separation -Presence in high CO_2 concentrations	-Cannot withstand high operating temperatures relevant to coal gasification processes	-Development of polymer materials that are stable at temperatures higher than 150°C -Development of hybrid materials for the separation of CO_2 from coal syngas

2.3 MEMBRANE PROCESSES INVOLVING ZEOLITES

2.3.1 ZEOLITE FRAMEWORK TYPES AND STRUCTURES

Zeolites are crystalline structures containing channels of angstrom size dimensions. These aluminosilicates are composed of tetrahedral building units interconnected with oxygen atoms of the form TO_4 (where T can range from Si, Al or P). Using these basic building blocks of T-atoms, all kinds of structures can be created with pores and

cavities of varying dimensions. These structures again govern other exploitable properties like ion exchange, sorption capacity, shape selectivity and their catalytic activity [11]. Information on the framework type can explain many of the observed properties of zeolites.

According to [11] there should be distinguished between framework type and framework structure for classification purposes. Framework type simply describes the topology of the framework's tetrahedrally coordinated atoms (T-atoms) in the highest possible symmetry. Here no reference is made to chemical composition, size and shape of pore openings, dimensionality of the channel system, volume and arrangement of the cages and the types of cation sites available as described by the framework structure in order to classify as many different materials under one designation. When describing the structure the influence of framework composition, extra-framework cations, organic species, adsorbed molecules and/or structural defects are considered.

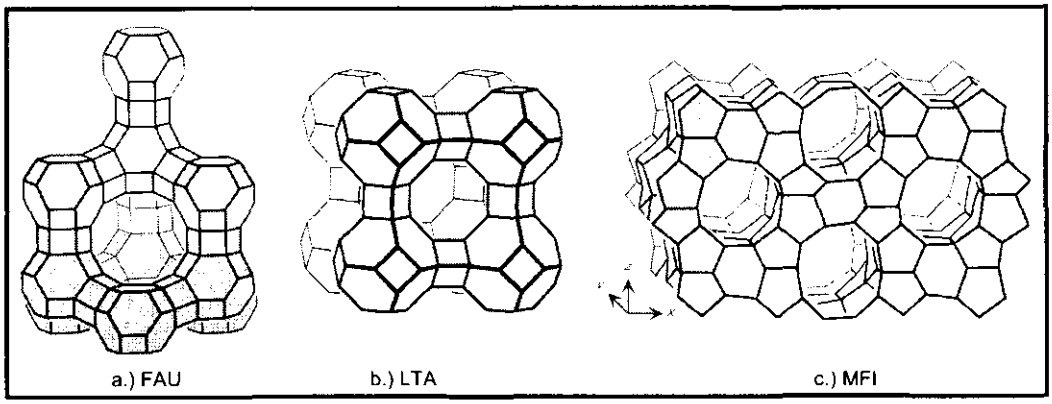

Figure 2-2: Different zeolite framework types (Taken from [11])

Figure 2-2 shows a view of the 136 [12] zeolite framework types confirmed by the Structure Commission. In this figure, the nodes represent T-atoms while the lines depict oxygen bridges. The FAU framework type consists of sodalite cages joined to one another via double 6-rings. This creates a so-called super cage with four 12-ring pore openings and a 3-dimensional channel system. For the LTA framework type the sodalite cage is a primitive cubic arrangement joined via double 4-rings. This leads to a α-cage in the centre of a unit cell and a 3-dimensional, 8-ring channel system. LTA

is one of the more open framework types with a framework density of only 12.9 T-atoms/1000 $Å^3$. The framework type of the high silica ZSM-5 zeolite is shown in Figure 2-2 c.). This framework is described in terms of [5^4] units linked to form pentasil chains. Identical images of these chains are used to connect to 10-ring holes forming corrugated sheets. The oxygen linked bridges to the next form leads to a 3-dimensional structure with zigzag channels.

When looking at framework structure many interesting properties can be explained by the framework composition. Neutral zeolites exist when the framework consist solely of $Si^{4+}O^{2-}_4$ tetrahedra [10]. In this case an oxygen atom bridges two T-atoms and the zeolite is said to be hydrophobic. In the case of aluminium (valence 3+), the framework becomes negatively charged and is compensated for by a positive ion (Na^+, K^+ or Ca^{2+}) or proton, H^+. The presence of aluminium renders the zeolite hydrophilic and acidic and enables the zeolite framework to allow for ion exchange. The presence of these counter ions might also obstruct pores and lead to reduce pore sizes. In short, increasing the Si/Al ratio increases the hydrophobicity of the zeolite and decreases the number of cations needed to balance the charge. Table 2-2 shows some of the characteristics of zeolites used in membrane applications.

Table 2-2: Characteristics of zeolites used as membranes (Adapted from [10])

Zeolite characteristics used in membrane configurations		
Zeolite	**Structure**	**Nature**
NaA	LTA	Hydrophilic
KA	LTA	Hydrophilic
SAPO-34	CHA	Hydrophilic
Ferrierite	FER	Hydrophilic
Silicalite-1	MFI	Hydrophobic
ZSM-5	MFI	hydrophilic/hydrophobic
Mordenite	MOR	Hydrophilic
NaY	FAU	Hydrophilic
NaX	FAU	Hydrophilic

Figure 2-3 below predicts the molecular sieving properties of the different types of zeolite structures by comparing typical zeolite pore sizes to the kinetic diameters of different molecules. For the three important species (H_2, CO_2 and CO) in this study it

can be predicted that LTA-type membranes like NaA will exhibit separation based on size differences, although the effect of adsorption should be investigated.

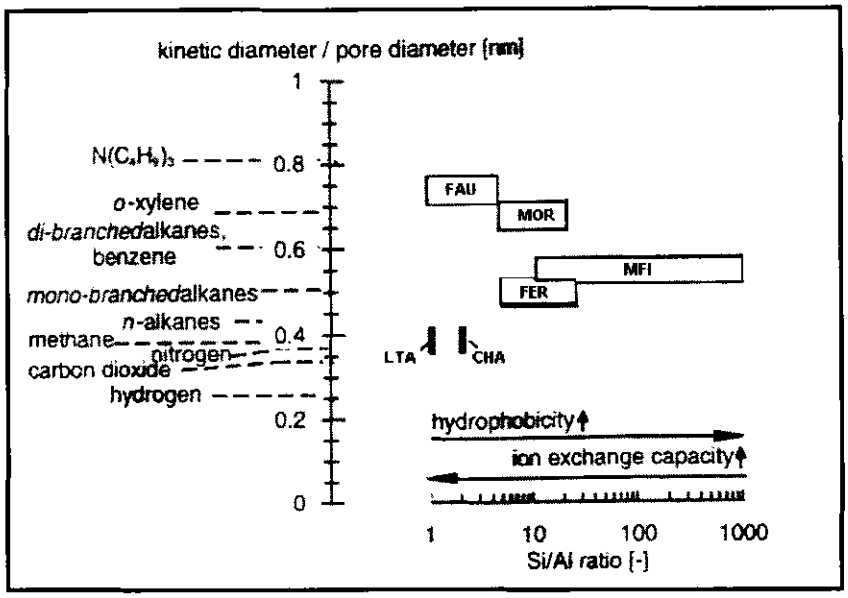

Figure 2-3: Separation applications for different zeolite structures (Taken from [10])

2.3.2 ZEOLITES IN H_2, CO_2 AND CO SEPARATION

NaA

Xu *et al.* [13-15] synthesized a NaA zeolite membrane onto a porous α-Al_2O_3 support. Permeation experiments were carried out with H_2, O_2, N_2 and n-C_4H_{10} and exhibited the same trend as in Figure 2-6 where the permeability decreased as molecular size was increased. H_2 permeability rates of 204 x 10^{-8} mol.m^{-2}.s^{-1}.Pa^{-1} at 25 °C were achieved compared to the 790 x 10^{-8} mol.m^{-2}.s^{-1}.Pa^{-1} achieved by [16] at the same temperature. Zhu *et al.* [17] showed that the permeability of gaseous components was strongly suppressed by the presence of water, resulting in high selectivities for water removal in the presence of gases like H_2, CO and CH_4. Figure 2-4 shows the permeability of single components through the zeolite 4-A membrane synthesized by Zhu *et al.* [17].

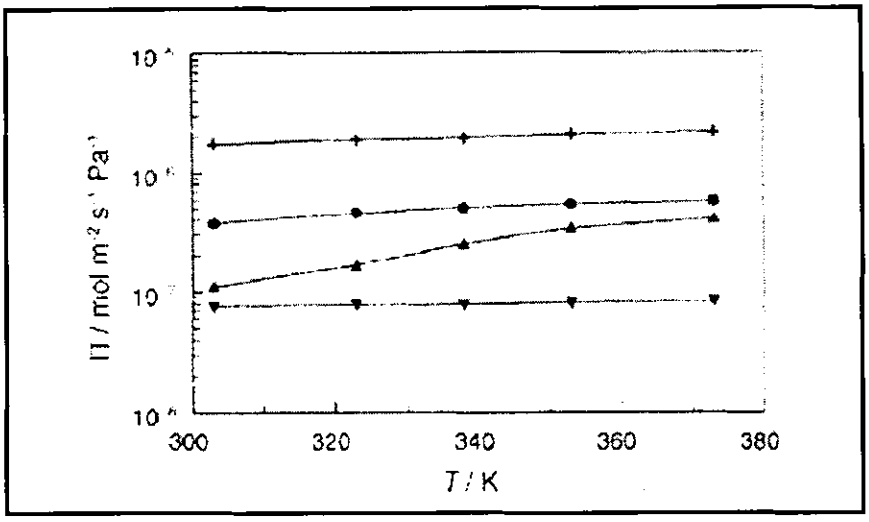

Figure 2-4: Unary permeability as a function of temperature according to the Wicke-Kallebach method for (+)H_2O, (▲)CO, (●)H_2 and (▼)CH_4 (Taken from [17])

Silicalite-1

The majority of zeolite-based studies using either H_2, CO_2, CO are conducted on MFI-type membranes such as silicalite-1 [16, 18-24]. Bakker *et al.* [18] reported the one-component steady-state permeation of gasses through a silicalite-1 composite membrane (on a stainless steel (SS) support) at temperatures ranging from 190 to 680 K. Gasses were studied in three groups; noble gasses, inorganic molecules and light hydrocarbons. The relevant molecules to this study were H_2, CO_2, CO (with these being the experimental gasses of this study), N_2 and SF_6 (with N_2 being used for characterisation purposes and SF_6 used to detect defects in the membranes).

Permeabilities for these gasses are studied as function of temperature according to the concentration gradient method (CGM) and show a clear maximum for CO_2 and CO, while that of H_2 seem to increase beyond 700 K as can be seen in Figure 2-5 below. These maxima can be described by equilibrium adsorption and activated surface diffusion, while a minimum occurs because the equilibrium amount adsorbed in a pore vanishes [18]. A similar trend was obtained for CH_4 by Van den Broeke *et al.* [19] at comparable conditions.

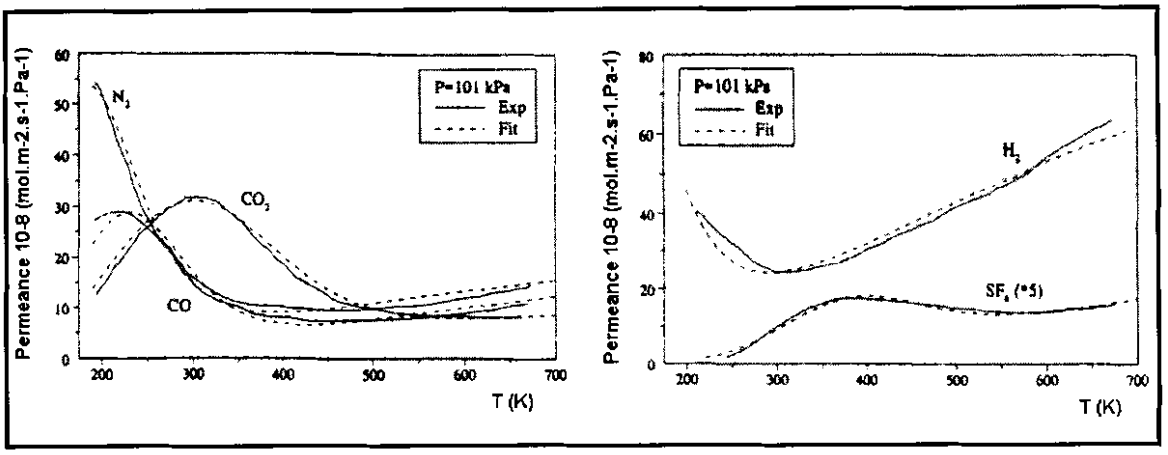

Figure 2-5: Permeability of inorganic gasses as a function of temperature (Taken from [18])

The permeability (at 673K) as a function of kinetic diameter is shown in Figure 2-6. Here it can be seen that the permeability decreases with increasing molecule size.

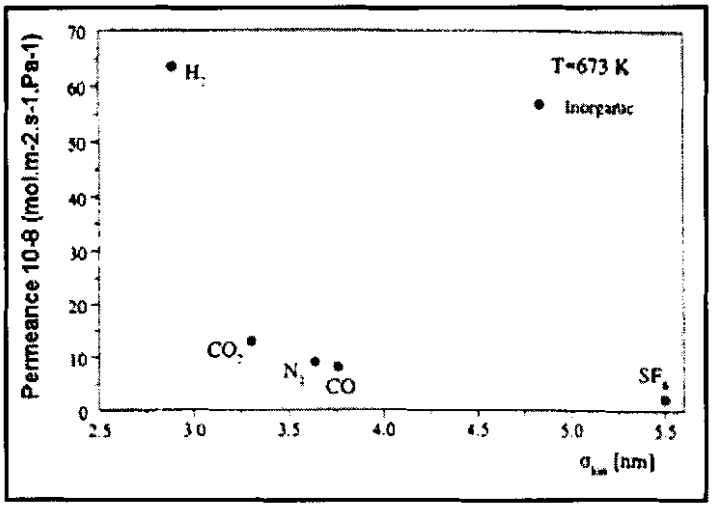

Figure 2-6: Permeability as a function of kinetic diameter (Taken from [18])

In another work, Bakker *et al.* [20] present binary permeation data for H_2 and CO_2 as shown in *Figure 2-7*. Here it is clear that CO_2 preferentially permeates at low temperatures with a high selectivity of about 12 at room temperature. This selectivity steadily declines to a point at 420 K where it inverts towards selectivity for H_2.

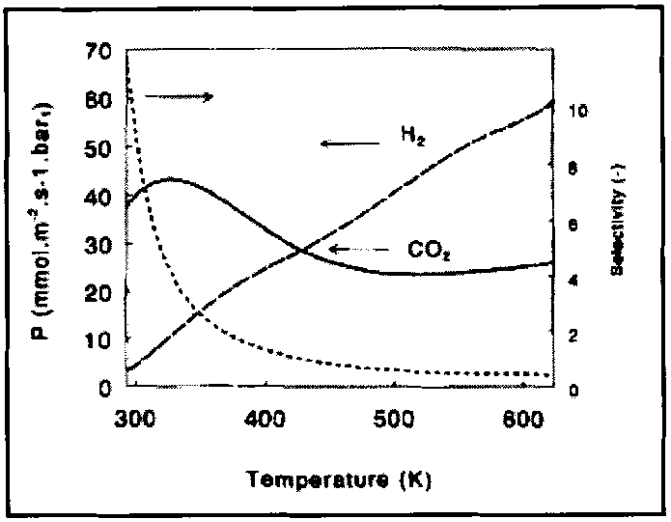

Figure 2-7: Permeability of a 50/50 mixture of H_2 and CO_2 as a function of temperature with TMP ≈ 40 kPa (Taken from [20])

Algiri *et al.* [16] reported unary flux data using silicalite-1 membranes as shown in *Figure 2-8*. In this case, the membranes differed in the sense that α-Al_2O_3 supports were used as opposed to the SS-supports used by [18]. From the data it is clear that the trend in permeation differs when compared to *Figure 2-5*. Here permeability shows a steady decline with increasing temperature for H_2, CO_2, and CO, while the work of Bakker *et al.* [18] shows distinct minima and maxima (in the cases of CO_2 and CO).

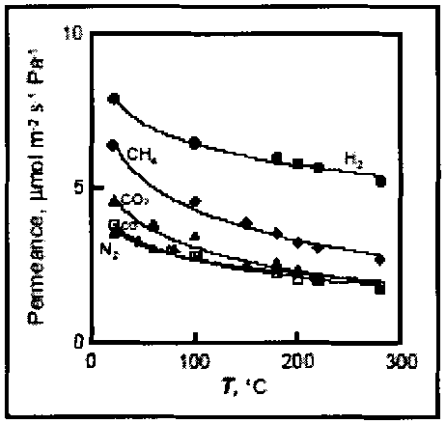

Figure 2-8: Permeability of pure gases as a function of temperature with TMP ≈ 40 kPa (Taken from [16])

[16] also conducted experiments with the pressure drop method (PDM). Permeation fluxes were studied as a function of trans-membrane pressure differences at room temperature, 100 and 220°C. The results are shown in Figure 2-9 below.

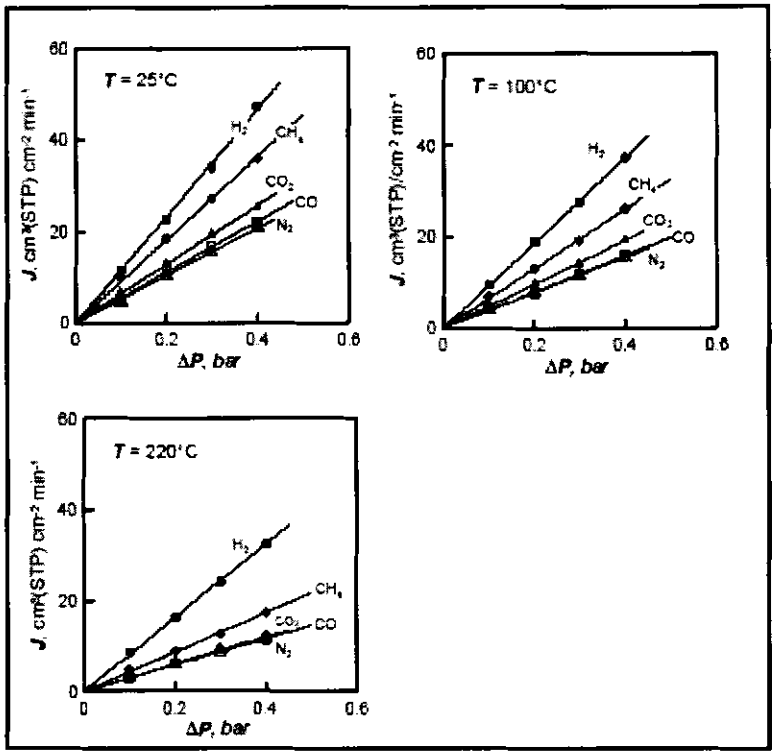

Figure 2-9: Permeation flux as a function of trans membrane pressure (Taken from [16])

Compared to the work of [18] (Figure 2-5 above), this data shows permeability differences of an order of magnitude. Table 2-3 below summarises some of the data from different studies. These results show the comparison for weakly adsorbing species (on silicalite) like H_2 and N_2 and the strongly adsorbed specie CO_2. From the table it can be concluded that the large difference in permeability between [18] and [16] is probably due to the large difference in membrane thickness.

Table 2-3: Comparison of unary permeation data for silicalite-1 membranes (Adapted from [16])

Zeolite/support shape	Thickness (μm)	T (°C)	ΔP (kPa)	Method	Permeability (μmol.m^{-2}s^{-1}Pa^{-1})		
					H_2	CO_2	N_2
Silicalite-1/α-Al_2O_3 (tube)	2	25	40	PDM	7.9	4.3	4.6
	2	200	40		5.8	3.2	1.9
Silicalite-1/SS (tube)	50	25	-	PDM	0.25	0.31	0.15
Silicalite-1/γ-Al_2O_3 (tube)	3	25	25	CGM	0.096	0.086	-
	3	200	200		0.15	0.034	-
Silicalite-1/α-Al_2O_3 (tube)	5	25	60-100	PDM	3.4	-	-
Silicalite-1/α-Al_2O_3 (disk)	0.5	25	80	PDM	21.9	-	12.9

Kapteijn *et al.* [21] studied the effect of a binary mixture of H_2/n-C_4 and found that, despite the much larger single component fluxes for H_2, the larger molecules would permeate faster after a given time. This phenomenon was attributed to the different adsorption characteristics of the molecules in silicalite-1. Van den Broeke *et al.* [22] also reported this behaviour. They found that for weakly adsorbing species the binary fluxes are similar to one-component fluxes. In the case of moderately or strongly adsorbed specie in the presence of such a weaker component, the flux of the weaker adsorbed component is greatly reduced.

ZSM-5

Literature on ZSM-5 zeolites, with regard to the experimental gasses used in this study, is limited to H_2/i-C_4H_{10} experimentation by Ciavarelle *et al.* [25], single component H_2 and CO_2 experiments by Geus *et al.* [26] and Hedlund *et al.* [27].

Ciavarelle *et al.* [25] prepared a composite alumina-MFI membrane. In contrast to [18], H_2 permeation decreased with increasing temperature. This behaviour was also shown by [24] for alumina supports.

Geus *et al.* [26] used ceramic supports to grow polycrystalline films of 50 to 80 μm of ZSM-5 membranes. These membranes gave unary fluxes of the same order as [15] despite the fact that the zeolite layers were more than 25 times larger.

Hedlund *et al.* [27] used α-alumina supports to grow 1.5 μm ZSM-5 films free of organic templates using a seeding technique. Single gas permeation experiments showed a decrease in permeation as the kinetic diameters increased as shown in *Figure 2-10.* This was also concluded by [18] with the only difference being that the temperature of the experiments (298 K for [27] and 673K for [12]). Results also differ by an order of magnitude for H_2 and CO_2 and about two orders for N_2.

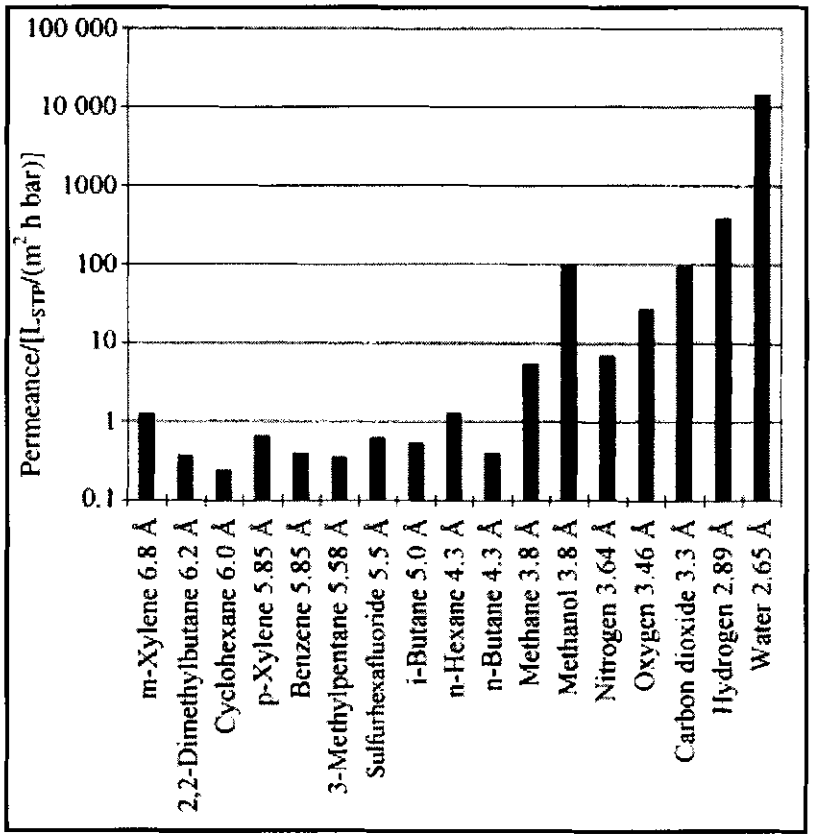

Figure 2-10: Permeability and kinetic diameter of different molecules in single gas experiments at a temperature of 145°C and 1 bar pressure (Taken from [27])

Other Zeolite Types

Various other zeolite types [23-30] were also used in experimentation, but rather focused on other aspects and/or gasses than the previous literature. The important outcomes are discussed below.

Hasegawa *et al.* [28] made use of an α-alumina tube as support with a NaY membrane synthesized onto the outer surface. The zeolite tube was ion-exchanged with solutions of either KCl, RbCl or CsCl. Single component permeation experiments were conducted at 35°C with CO_2 and N_2. A maximum permeability of 3 x 10^{-6} $mol.m^{-2}.s^{-1}.Pa^{-1}$ was reported for CO_2, which is about an order of magnitude higher than the permeability reported by [16, 26].

Nishiyama *et al.* [29] used MOR and FER membranes to test the permeability of H_2, He, CH_4, N_2, O_2 and CO_2 at temperatures ranging from 290 – 400K. The permeabilitys for most of the gasses were about 100 times greater through the MOR-type than through the FER-type. This is due to the larger pore sizes associated with MOR (*see Figure 2-3)* membranes.

Gas separation experiments were also conducted with DDR-type zeolite membranes on alumina supports by Tomita *et al.* [30]. In these experiments single component fluxes were plotted against absolute feed pressure (varied from 0.1- 0.6 MPa) and exhibited the same linear characteristic as in Figure 2-9.

2.4 QUANTIFYING TRANSPORT IN ZEOLITE MEMBRANES

2.4.1 INTRODUCTION

Transport in microporous membranes can be described in five consecutive steps [31]. These steps involve intracrystalline and interfacial processes. The sequence of events takes place as depicted in Figure 2-11:

1. Adsorption from the gas phase onto an external surface
2. Transport from the external surface into the zeolite pores
3. Intracrystalline transport/diffusion
4. Transport from the zeolite pores to the external surface
5. Desorption from the external surface to the gas phase

Steps 1, 2, 4 and 5 are known as interfacial processes, while step 3 is referred to as an intracrystalline process. These are all activated steps and can be modelled by assuming that molecules move between low-energy sites [10]. Each move is correlated to activation energy and the net flow is determined from the product of forward and reverse motion. The rate-determining step is determined by the operating conditions, the characteristics of the molecule and the crystalline material.

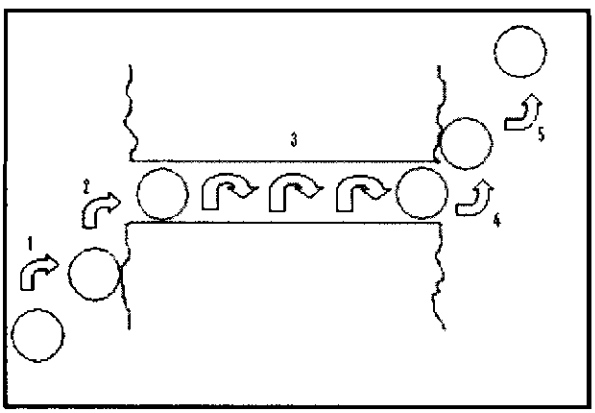

Figure 2-11: Five-step model for mass transfer through a zeolite membrane [31]

From the model, the following conclusions can be drawn [20]:

- Steps 1 and 5 will depend on the conditions of the gas phase on either side of the membrane.
- Adsorption on the external surface for weakly adsorbing species at high temperatures will not occur.
- Molecules that enter directly from the gas phase will have to move at a right angle to prevent them from bouncing back.
- In general, bulky molecules will enter pores with more difficulty than small ones
- In the region of strong adsorption and high occupancies, molecules will exhibit strong interactions.
- Interactions among molecules will affect diffusional behaviour.

Intracrystalline diffusion (step 3) is also described as configurational (as described by [32]) diffusion, where molecules move from one adsorption site to another in the zeolite pore. With increasing temperature, the kinetic energy of the molecules increases, while interactions with adsorption sites remain constant. Above a certain temperature, no adsorption will take place. Consequently, transition from configurational diffusion toward Knudsen-diffusion (in which mass transport is kinetically determined) can occur.

2.4.2 INTRACRYSTALLINE DIFFUSION

Permeation through membranes is quantified with permeability. This is the flux through the membrane divided by the trans membrane pressure (ΔP_i).

$$\Pi_i = \frac{J_i}{\Delta P_i} \tag{2.2}$$

In the absence of capillary condensation, five types of transport mechanisms of gases and vapours can be distinguished in diffusion through zeolite membranes [10]:

1. **Viscous flow**: Convective flow in the direction of an absolute pressure gradient. This diffusion is strongly related to pore size.

$$\Pi_i = \frac{1}{R.T}\frac{g}{\Delta x}\frac{r_p^2}{8.\eta_i}\overline{P_i} \qquad \text{with} \quad \eta_i \propto T$$

$$\Pi_i \propto T^{-2}, P_i \qquad \textbf{(2.3)}$$

2. **Bulk or molecular diffusion**: Molecule-molecule collisions in the gas phase. It becomes important for large pore diameters or high system pressures. This type of diffusion does not contribute to single component systems.

$$\Pi_i = \frac{1}{R.T}\frac{g}{\Delta x}D_{ij} \qquad \text{with} \quad Dij \propto T^{1.75}, P^{-1}$$

$$\Pi_i \propto T^{0.75}, P_i^{-1}$$

(2.4)

3. **Knudsen diffusion**: This diffusion is dominated by molecule-wall collisions. This mechanism is prevailing when the mean free path of the molecules is larger than the pore diameter (low pressures or high temperatures).

$$\Pi_i = \frac{1}{R.T}\frac{g}{\Delta x}D_i^{Kn} \qquad \text{with} \quad D_i^{Kn} \propto T^{0.5}$$

$$\Pi_i \propto T^{-0.5} \qquad \textbf{(2.5)}$$

4. **Surface diffusion**: Activated transport of adsorbed species along the pore wall.

$$\Pi_i = \frac{\rho.q_{sat,i}.g.D_i^s.\nabla \ln(1-\theta)}{\Delta p_i} \text{ with} \quad D_i^s \propto \exp\left[\frac{-E_{a,i}^s}{R.T}\right], \theta_i = f(T, p_i)$$

$$\Pi_i \propto f(T, p_i) \qquad \textbf{(2.6)}$$

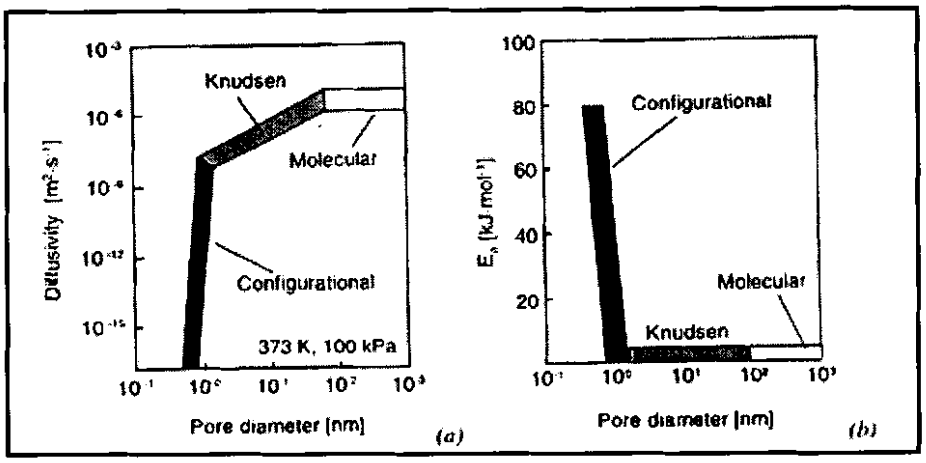

Figure 2-12: Effect of the pore diameter on diffusitivities (a) and on the activation energy for diffusion (b) (Taken from [10])

5. **Configurational diffusion**: During diffusion in micropores, molecules can either retain a gaseous character or adsorb on the micropore surface. In the latter case, diffusion is described by equation 2.8. Otherwise, activated gaseous diffusion takes place as described in equation 2.9.

$$\Pi_i = \frac{1}{R.T}\frac{g}{\Delta x}\sqrt{\frac{8.R.T}{\pi.M}}\exp\left[\frac{-E_a^g}{R.T}\right] \qquad \text{with} \qquad \Pi_i \propto f(T) \tag{2.7}$$

In these equations g is a geometrical factor that accounts for the porosity and tortuosity of the porous medium.

Flux or permeability in a porous membrane can be used to characterise the pore size of the membrane due to observed temperature and pressure dependencies. Figure 2-13 shows the temperature dependencies for the different diffusion regimes. Molecular and configurational diffusion shows an increasing trend with temperature, while a decrease is observed for Knudsen diffusion and viscous flow. For systems where surface diffusion exist shows a maximum as a function of temperature.

Looking at the pressure dependencies of the permeability, it is clear that transport according to viscous flow is the only mechanism that results in an increase in permeability with increasing pressure. Since this is only applicable to larger pores, viscous flow should be absent in micropores and can be used to measure the quality of microporous membranes. The permeability resulting from Knudsen and configurational diffusion is independent of pressure drop, while that of surface and molecular diffusion decreases non-linearly with increasing pressure. Interestingly, while the permeability of molecular diffusion decreases with pressure the flux remains constant. This is due to the fact that for the flux the increased trans-membrane pressure drop compensates for the decrease in diffusitivity with pressure. For surface diffusion, the flux increases non-linearly. This non-linear behaviour (for flux and permeability) is due to the non-linearity of adsorption in zeolites.

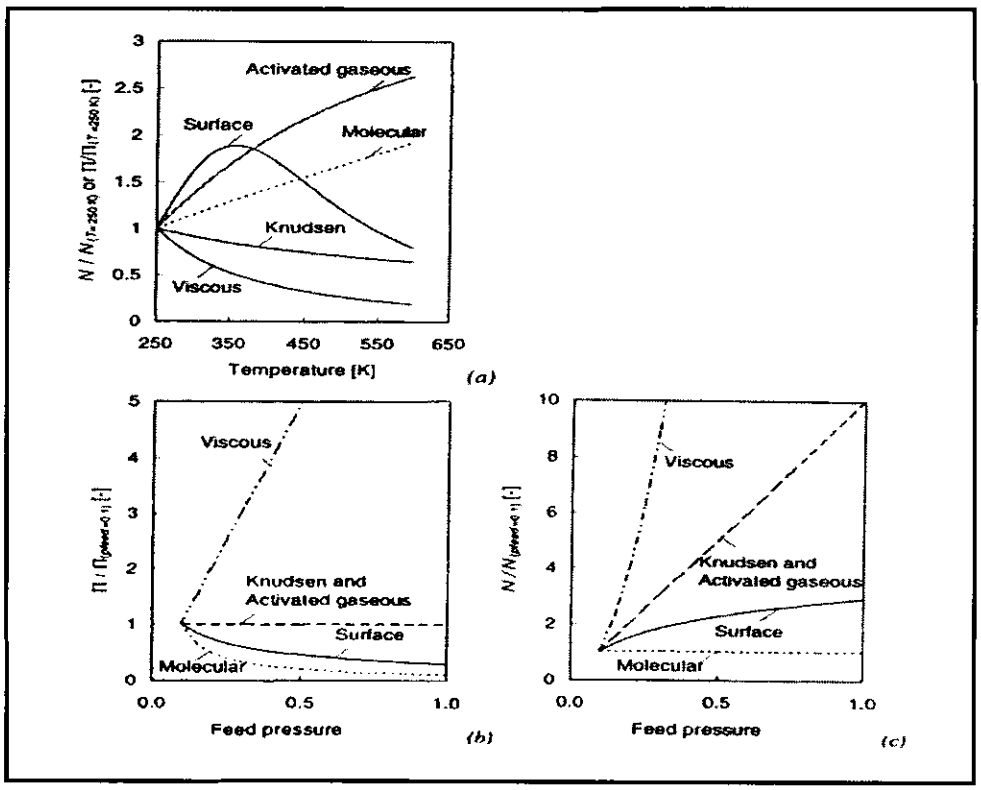

Figure 2-13: Trends in permeation and flux as a function of temperature (a) and feed pressure (b,c) (Taken from [10])

When characterising membranes permeability is a suitable quantity for weakly adsorbing species since it is independent of pressure drop. It can also be used to check for the presence of viscous flow. For adsorbing components, flux is a more convenient quantity for the interpretation of data due to the non-linear relationship between flux and trans membrane pressure.

2.4.3 TRANSPORT MECHANISMS AND MASS TRANSFER CONSIDERATIONS

During experimentation, the steady-state transport of single and multicomponent mixtures is measured and presented. There are different transport mechanisms to represent the different regions that exist within the composite system. Hanebuth *et al.* [33] concluded that not enough attention is given in literature to quantify additional influences to resistance. Two areas that are neglected include the resistance of the support layer and defects in the selective layer.

For the purpose of this study the effect of the support layer is taken into account by firstly identifying the relevant transport mechanism in the support and then relating that information to the pressure drop expected over the support layer.

In materials with relative large pore sizes (0.05 – 10 μm), three transport mechanisms for gasses should be considered: bulk diffusion, Knudsen diffusion and viscous flow. Bulk diffusion, which is dominated by molecule-molecule interactions, does not contribute in single component systems and will not be considered. The contribution of Knudsen diffusion can be evaluated based on the Knudsen number (K_N). K_N is a measure of the ratio of the mean free path between molecules and the size of the pore radius and is given by [10]:

$$K_N = \frac{16.\eta_i}{d_p.5.\pi.\bar{P}}\sqrt{\frac{\pi.R.T}{2.M_{w,i}}} \qquad \textbf{(2.8)}$$

The effect of Knudsen diffusion becomes more apparent as K_N tends to 1. From Fick's first law of diffusion it follows that:

$$J_i^{Kn} = D_{Kn}\frac{\Delta C}{\Delta x} = D_{Kn}\frac{1}{R.T}\frac{\Delta P}{\Delta x} \tag{2.9}$$

Where D_{Kn} is known as the Knudsen diffusion coefficient and can be expressed as:

$$D_{Kn} = \frac{2}{3}.\frac{\varepsilon}{\tau}.r_p.\sqrt{\frac{8.R.T}{\pi.M_{w,i}}} \tag{2.10}$$

And taking [8]:

$$\tau = \frac{1}{\varepsilon} \tag{2.11}$$

Equations 2.12 to 2.14 can be combined to give relationship for pressure drop across the support:

$$\Delta P_{\text{sup}}^{Kn} = \frac{J_i.R.T.\Delta x}{D_{Kn}} \tag{2.12}$$

In the transition region transport is governed by both Knudsen diffusion and viscous flow as shown by the relation:

$$J_i = J_i^{Kn} + J_i^{vis} \tag{2.13}$$

Viscous flow is the result of the absolute pressure drop and is given by:

$$J_i^{vis} = -\frac{1}{R.T}.\frac{\varepsilon}{\tau}\frac{r_p^2}{8.\eta_i}.\overline{P}.\frac{\Delta P_{vis}}{\Delta x} \tag{2.14}$$

Where $\overline{P}$ is the average pressure between the shell and tube side. Once the contribution of the support to the overall resistance is determined, it can be incorporated to accurately describe the permeability through the entire membrane.

$$\Pi_i = \frac{J_i}{\Delta P_{mem}} \tag{2.15}$$

In this case, ΔP_{mem} is the pressure drop across the membrane only. By subtracting this from the overall pressure drop, a more realistic value is obtained for Π_i:

$$\Delta P_{mem} = \Delta P - \Delta P_{sup} \tag{2.16}$$

In order to predict the selective properties of a membrane the Knudsen diffusion ratio can be used. This parameter is based on the square root of the ratio of the molecular weights of two species and gives an indication of separation that can be expected in a Knudsen governed transport regime [13]. The ratio is given by:

$$Kn_{A/B} = \sqrt{\frac{M_{w,B}}{M_{w,A}}} \tag{2.17}$$

CHAPTER 3: EXPERIMENTAL

3.1 INTRODUCTION

In this study gas separation is investigated in a zeolite membrane on a tubular α-alumina support. In particular, a comparative study will be done to determine the difference in gas permeation characteristics between a double and triple coated NaA membrane. To be able to do the permeation experiments a number of prior activities should take place. These activities are summed up below:

- Manufacturing of a tubular α-alumina support by centrifugal casting [34-36] and sintering using AKP-30 powder.
- Coating of the support with a NaA zeolite [6, 37].
- Characterisation of the zeolite membrane using gas permeation and SEM.

Finally, the experimental program will follow. This program will include permeation experiments with pure components (H_2, CO_2 and CO) and binary mixtures. During these experiments operating conditions like feed pressure, feed composition, mode of operation and temperature will be varied.

3.2 EXPERIMENTAL PROCEDURES

3.2.1 MEMBRANE PREPARATION

SUPPORT

The composite, tubular membrane used in this study consists of a thin zeolite layer on an α-alumina support. The support is manufactured from AKP-30 powder (Sumitomo Chemical Company, Ltd., Japan) with a particle size distribution of 1.5 wt % < 0.27 μm + 89 wt % < 1 μm and mean particle size of 0.62 μm. The BET surface area for

this powder is 3.5 m^2/g [35]. 20 ml of APMA (Ammonium PolyMethAcrylate aqueous solution, Darvan C, R.T. Vanderbilt Company, Inc., Norwalk, USA) and distilled water were mixed (120 ml in total) and were brought to pH=9.5 by adding concentrated ammonia. The suspension obtained from mixing this solution to 120 g of AKP-30 powder was ultrasonically treated for 15 minutes using a frequency of 20 kHz and transducer output of 100W (Model 250 Sonifier, Branson Ultrasonics Corporation, Danbury, USA).

This suspension was then poured into a 6 cm stainless steel mould (precoated with a solution of Vaseline in petroleum ether on the inside to ensure easy mould release) that is rotated by a custom-build centrifuge (*see Figure 3-1*) for 20 minutes at 20 000 rpm. After pouring off excess liquid the support was dried inside the mould for a day at 30°C. The support was then removed from the mould and sintered horizontally on a flat surface at 1100°C for 1 hour with a heating and cooling rate of 1°C/min.

MEMBRANE

The NaA membrane was produced from a mixture of sodium metasilicalite pentahydrate ($Na_2SiO_3:5H_2O$ BDM), sodium aluminate (0.41 Na_2O, 0.54 Al_2O_3 Riedel-de Haën), sodium hydroxide (0.97, Aldrich) and MilliQ water. These ingredients were used in a molar oxide composition ratio of $48.9Na_2O:Al_2O_3:5.08SiO_2:979.2H_2O$.

First, an alumina solution was prepared by adding 4.807g NaOH and 20g H_2O together and stirring the solution until all the NaOH was dissolved. This was followed by the addition of 0.452g $NaAlO_2$ and stirred for 1 hour. Co-currently, to this, a silica solution was prepared by adding 3.481g NaOH to 20g H_2O and stirring the solution until all the NaOH was dissolved. Here 2.628g $Na_2SiO_3:5H_2O$ was added and stirred for an hour.

Afterwards, the alumina solution was added dropwise to the silica mixture while continuously stirring the mixture. The resulting clear solution was left to age for 30 minutes at room temperature. 15 ml of this solution was added to an autoclave

containing the finished support fitted into a Teflon tube. The autoclave rotated the solution containing the support for 30 minutes at room temperature before the actual synthesis for 3.5 hours at 358 K. The rotating autoclave was left to cool down at room temperature for another 3 hours. The composite membrane was separated from the remaining solution and thoroughly rinsed with MilliQ water. The membrane was then sonicated in MilliQ water at intervals of 10 minutes for an hour. This is needed to remove loose zeolite crystals. For additional coatings, a similar procedure is required. The difference lies in the fact that the aging time for the aluminium-silicate solution becomes an hour and that the autoclave was immediately heated to 358 K. Sonication in MilliQ water is done 3 times for 6 minutes each.

The values and settings above were taken from [6], as these conditions yielded the optimum membranes used in pervaporation experiments using Ethanol-Water mixtures.

3.2.2 EXPERIMENTAL APPARATUS

Various pieces of equipment are used during the preparation and characterisation of the support, preparation and characterisation of the NaA membrane and the actual permeation experiments. They will be discussed below:

SUPPORT MANUFACTURE

Following paragraph 3.2.1, equipment used to prepare supports includes an ultrasonic bath, stainless steel moulds, a custom build centrifuge *(see Figure 3-1)* and a sintering oven.

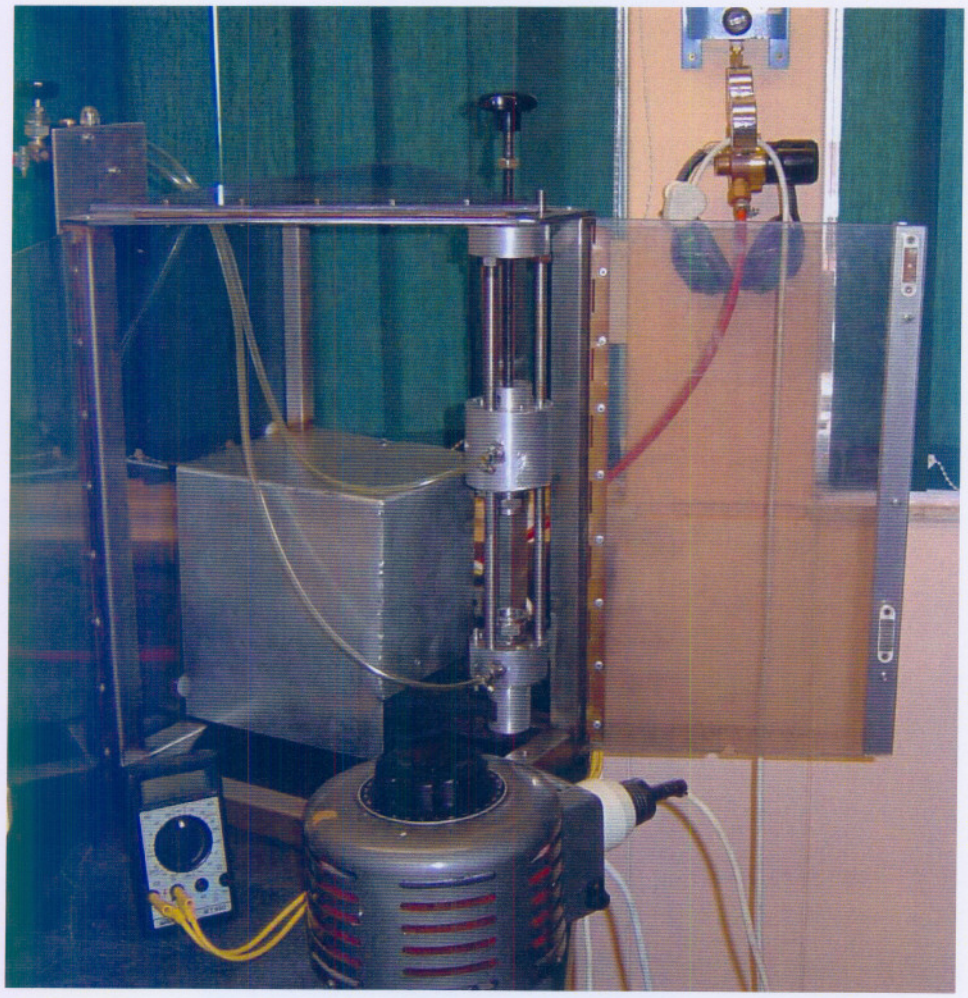

Figure 3-1: Custom built centrifuge for support manufacture (Taken from [36])

MEMBRANE MODULE

The membrane is housed in a stainless steel module that consists of two circular flanges at the ends and an outer sleeve that encapsulates the membrane as shown in Figure 3-2.

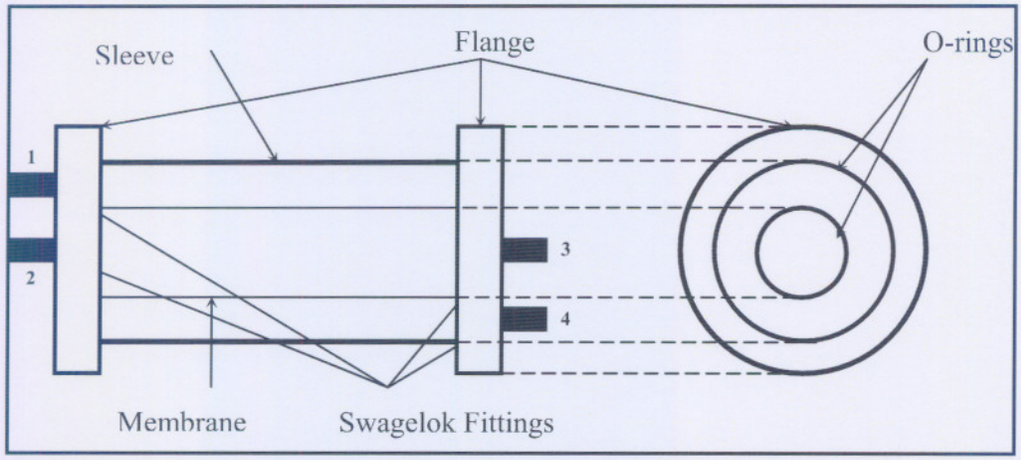

Figure 3-2: Schematic drawing of membrane module (and fitting positions) with a side view of the assembled module on the left and a top view of the flange head on the right.

Swagelok fittings are fitted to the flanges where line connections are made for the feed, sweep, permeate and retentate lines. When a sweep gas is not used the relevant lines are simply blocked by a blanked off fitting.

Both the membrane and module sleeve is sealed at the ends (on the heads) with Viton o-rings. The module is tightly closed using the high tensile steel bolts as in Figure 3-3.

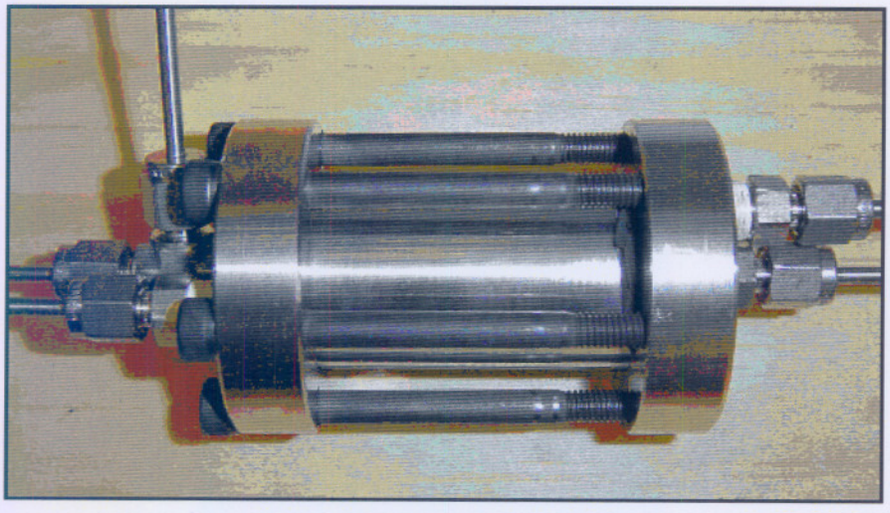

Figure 3-3: Membrane module

GAS PERMEATION

The gas permeation setup is shown in Figure 3-4 below. Single and binary gas mixtures of H_2 (Afrox > 99.99% pure), CO (Afrox, 99.99%) and CO_2 (Afrox, 99.5%) are made up using the mass flow controllers *(Brooks Instrument, Model 5850 TR)*. A tube furnace *(Lenton Furnaces, LTF14/50/180 Vertical)* is used to regulate the module temperature. A thermocouple is inserted into the membrane module (Typically at position 2 when looking at Figure 3-2. This section corresponds to the T-piece that can be seen on the left of Figure 3-3) and is connected to the temperature controller that forms part of the Lenton Furnace. A 1 m piece of coiled stainless steel tubing precedes the module (also inside the furnace) to ensure that the temperature of the feed gas is at oven temperature. Two backpressure regulators *(Swagelok, LP.0-500psig)* are used to regulate the feed and trans membrane pressures. A custom-made soap flow meter is used to determine the permeate and retentate flow rates, while gas analysis is done on a gas chromatograph *(Varian Star 3400 GC with SUPELCO CARBOXEN 1010 PLOT FUSED SILICA Capillary Column, 30m x 0.32mm)*.

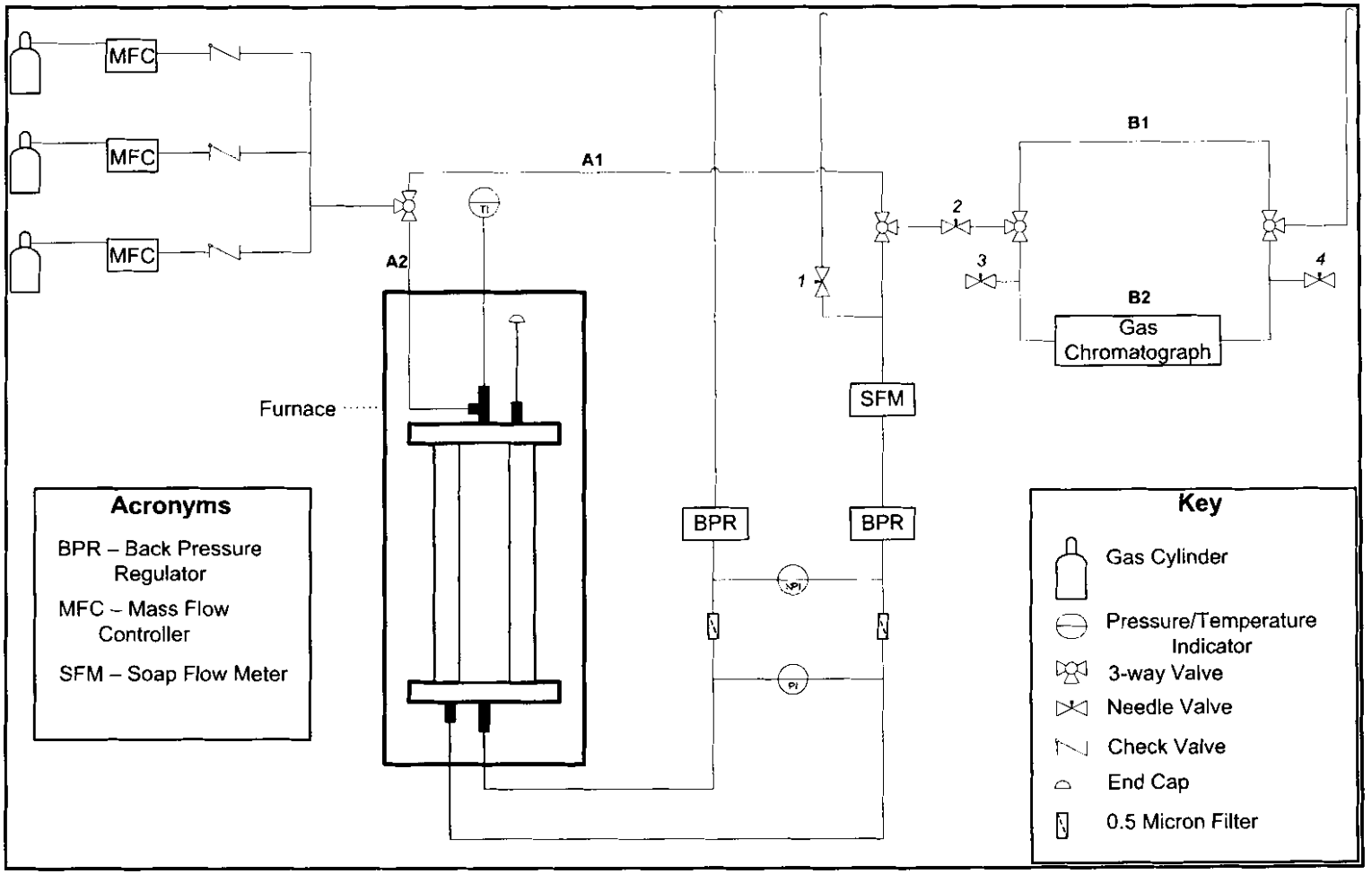

Figure 3-4: Process flow diagram

3.2.3 EXPERIMENTAL PROCEDURE

Gas permeation experiments are carried out in two ways, according to the different modes of operation discussed in paragraph 2.1 *(also see Figure 2-1)*. For membrane characterisation, dead-end mode is employed at 25°C with pressure differences ranging from 0.5 to 2.0 bar. This method is also used throughout the experimental cycle to validate membrane integrity and reproducibility of experimental data.

Permeation experiments however were conducted in cross-flow mode. These experiments can be divided into two main groups namely unary/single flux/permeation experiments and binary flux/permeation experiments. For each of these groups the effects of temperature, feed composition, feed flow rate and feed pressure were investigated.

Following the logic in Figure 3-4 above, 4 main gas routes can be identified. These are A1, A2, B1 and B2. A1 is essentially a bypass route that is used when a reference gas is send to the GC. A2 is the main gas flow through the membrane module. B1 and B2 are used to either vent or send gas to the GC. For single gas permeation experiments, only A1 is used while binary experiments make use of all the routes. A detailed experimental procedure is given in Appendix C. For each experiment the permeate flow rate was measured using a soap flow meter and the flow rate recorded. This was a value with unit ml/min and was converted to molar flow rate using the relation:

$$P.\phi_v = \phi_m.R.T \tag{3.1}$$

The molar flow rate was converted to molar flux using:

$$J_i = \frac{\phi_m}{A} \tag{3.2}$$

where A is the membrane surface area and is given by:

$$A = \pi.d.l \tag{3.3}$$

From the flux the permeability can be determined by equation 2.5.

CHAPTER 4: RESULTS AND DISCUSSION

4.1 INTRODUCTION

Two different membranes are used in this study: a double and triple coated NaA membrane. The triple coated membrane will form the primary focus of the study and reference to the double-coated membrane will be made in cases where comparisons are made. For convenience, M2 will refer to the double coated membrane while M3 will be used as reference for the membrane with the triple coating.

4.2 CHARACTERISATION OF SUPPORT

The support used for the membranes in this study is manufactured from an AKP-30 powder supplied by Sumitomo Chemical Company Ltd. The important characteristics of the prepared support (sintered at 1100°C) are given in the table below:

Table 4-1: Support properties and dimensions [36]

Property		Value - Unit
Tube side radius	r_t	8.89 mm
Shell side radius	r_s	10.39 mm
Length of support	l	56.10 mm
Porosity	ε	0.396
Average pore radius	r_p	52.40 nm

The dimensions r_t, r_s and l were determined with a Vernier while ε and r_p were determined by mercury porosimetry [36]. Support characterisation was based on five main activities:

1. The physical support dimensions and linear shrinkage.
2. Mercury porosimetry
3. Water permeability

4. SEM
5. Strength test

In order to determine the linear shrinkage that occurred during sintering a distance of 49.8 mm was marked on the unsintered cast after it has been dried. This distance was then measured again after sintering using a Vernier and the corresponding percentage decrease calculated. It was found that the dimensions were influenced by the temperature as well as the particle size of the powder [36]. For the given support, the linear decrease/shrinkage was calculated at 1.61%.

As stated above, ε and r_p were determined by mercury porosimetry (Autopore III, Micrometrics) and is given in Table 4-1 above. Samples were dried at 120°C for 6 hours or more to remove any moisture present in the crystalline structure. Analysis was conducted with a penetrometer (Part number 942-61707-00) which had a total stem volume of 0.392 cm^3. Between 60% and 90% of this volume was utilized under high pressure intrusion.

Water permeability was used to obtain experimental data that could be used and tested against the theoretical data (obtained from the mercury porosimetry) in order to verify the results. [36] found that the water permeability experiments produced a flux of 0.260 $mol/m^2.s.bar$ while the theoretical flux was calculated at 0.205 $mol/m^2.s.bar$. This is an indication that the parameters shown in Table 4-1 are of the correct order.

Destructive strength tests were used to exert pressure on the inside of the tubular structure until breakage occurred. The given support was capable of withstanding internal pressures of up to 760 MPa before breaking. Furthermore, [36] observed a linear increase in mechanical strength as a function of sintering temperature and that an inverse relation exists with porosity.

4.3 SINGLE GAS PERMEATION THROUGH A SUPPORTED ZEOLITE MEMBRANE

4.3.1 DEAD-END EXPERIMENTATION

As concluded by Zhu *et al.* [17], the permeability of gases like H_2, CO and CH_4 through a zeolite-4A membrane is strongly influenced by the presence of water. In the case of a "wet" membrane, almost no permeation could be detected using the dead-end method *(described in Appendix C)*. Therefore, a "dry" membrane was needed for experimentation. The results are shown in Figure 4-1. To ensure that a membrane was

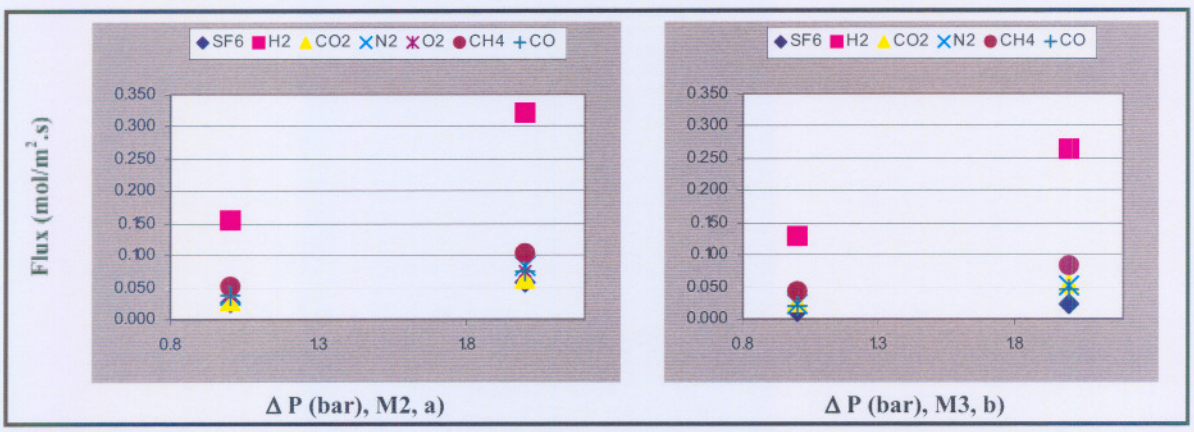

Figure 4-1: Gas permeability of a "dry" membrane, a) M2 and b) M3 at 25°C

always dry, it was heated (at 1°C/min) to 100°C and kept there for 3 hours before a series of experiments. The figures show that the flux increases with increasing pressure drop across the membrane. It can also be noted that higher fluxes are obtained with M2, which is expected due to the addition of an extra resistance layer in M3. Another note is the fact that the flux on average almost doubles for the increase in pressure drop from 1 to 2 bar. Table 4-2 gives a comparison of the fluxes through M2 and M3 at pressure differences of 1 and 2 bar (at room temperature). SF_6 shows the lowest percentage changes (from M2 to M3) while H_2, CO_2 and CH_4 show similar values. As mentioned in *paragraph 3.2.3* this method is also used to validate membrane integrity throughout the experimental cycle. In addition it is also used as

the basis for the reproducibility of results. After each set of experiments where completed (and the membrane was dried) such a experiment was carried out and compared to the baseline (*Figure 4-1*). Results never varied with more than 8%.

Table 4-2: Permeability comparison for M2 and M3 at T = 25°C and ΔP at 1 and 2 bar

Component	Flux (mol/m^2.s)		Pressure (bar$_g$)	$\frac{M3}{M2}.(100)$
	M2	M3		
SF_6	0.057	0.024	2	41.2
	0.025	0.011	1	42.9
H_2	0.322	0.265	2	82.1
	0.156	0.128	1	82.3
CO_2	0.064	0.053	2	82.6
	0.028	0.025	1	88.1
N_2	0.082	0.051	2	62.6
	0.037	0.024	1	64.1
O_2	0.075	-	2	-
	0.038	-	1	-
CH_4	0.105	0.085	2	80.8
	0.053	0.044	1	83.6
CO	0.076	0.045	2	59.8
	0.038	0.021	1	56.8

Figure 4-2 shows the gas permeability as a function of kinetic diameter. In graph b) the same general trend shown by [13 – 17, 18] can be observed. This is an indication of the molecular sieving effect of M3.

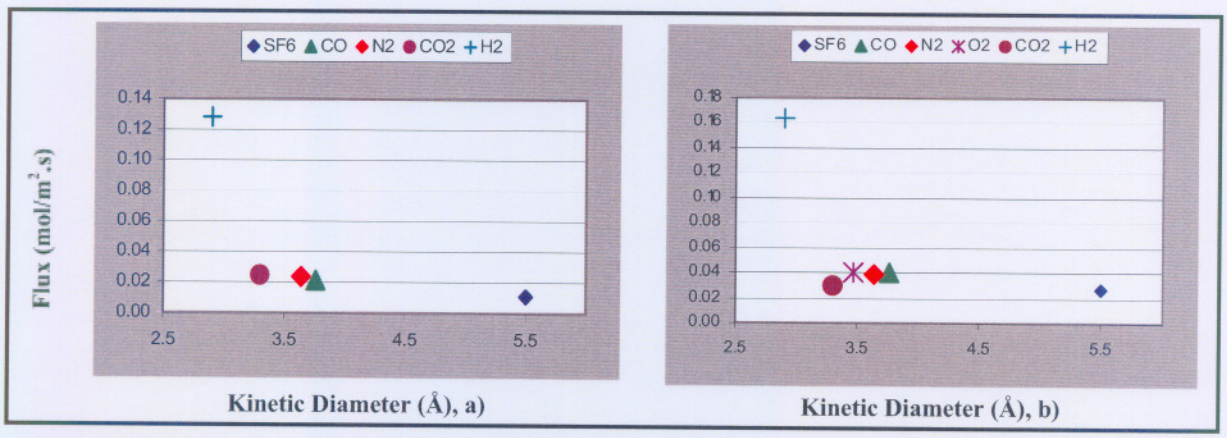

Figure 4-2: Gas flux as a function of molecular kinetic diameter at 25°C and ΔP = 100 kPa for a) M2 and b) M3

Considering the nature and properties of NaA the ideal flux of H_2/SF_6 can be used to determine the perfection of the membrane. Because the kinetic diameter of SF_6 (5.5 Å) is larger than that of the NaA pores, SF_6 should not permeate through a defect free membrane. Defects in membranes are non-selective pathways that form in parallel with membrane pores. These defects can be observed as cracks or gaps between zeolite crystals. Another form of non-selective pathways is the presence of grain boundaries between adjacently grown zeolite crystals [38]. These boundaries are inherent to membrane structure due to its polycrystalline nature and can extend over the entire zeolite film. As a result, intercrystalline pathways that contribute to transport across a membrane exist. [39] and [40] also gives reference to this phenomenon while Nelson *et al.* [41] mathematically explains the difference between perfect and imperfect membranes using the Langmuir model for single component permeation. [41] also showed that the spacing of defects or grain boundaries can have a large effect on the flux.

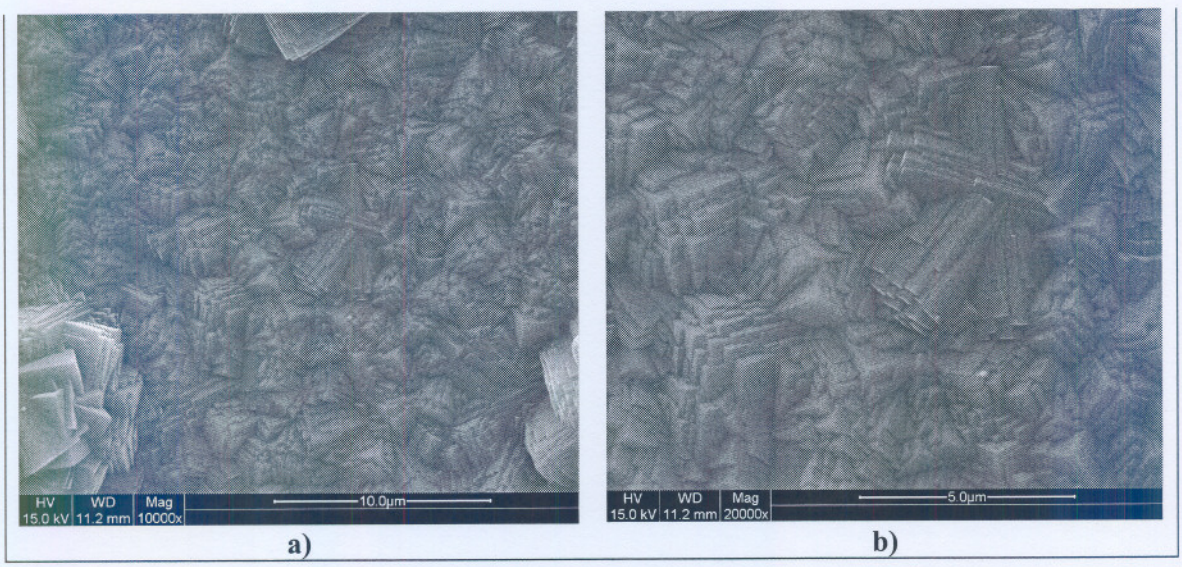

Figure 4-3: SEM photos of the NaA layer in M3 at different magnification; a) 10000 and b) 20000

Figure 4-3 shows the SEM photos of the surface condition of M3. In both a) and b) numerous crystal growth directions can be identified which suggest that various grain boundaries can exist in M3. Although membranes prepared according to the same recipe showed good selectivities for pervaporation, it can also be seen that crystal

grow is not completely finished. A recent study, on the influence of synthesis time on crystal growth has shown that a synthesis times of 4, instead of 3.5 hours, has to be used for complete formation of crystals [6]. The presence of SF_6 transport through zeolite membranes is shown in Figure 4-2 and is also reported by other authors [18, 33].

The permselectivity of H_2/SF_6 can be used to predict the selective properties of M2 and M3. The higher this ratio the higher the probability that separation will occur in the binary mixture, although differences in adsorption characteristics may prove otherwise [21 – 22]. The effect of intercrystalline diffusion can be associated with the case where this selectivity becomes close to or lower than the Knudsen diffusion. Table 4-3 gives a comparison between this ratios and permselectivities for the various gases shown in Figure 4-2. These results support the observation regarding the presence on intercrystalline diffusion and it can be expected that separation will be limited to the Knudsen diffusion ratio.

Table 4-3: Comparison between Knudsen diffusion ratios and ideal fluxes for various gases at 25°C and ΔP = 1 bar

Compared Gases		**Knudsen Diffusion Ratio**	$\frac{Ji}{Jj}$	
i	j		**M2**	**M3**
H_2	SF_6	8.50	6.11	11.73
H_2	CO	3.72	4.15	6.02
H_2	CO_2	4.67	5.58	5.22
H_2	N_2	3.72	4.23	5.44
CO_2	CO	1.66	0.74	1.15

The table above predicts that for an increase in resistance (in the form of the extra zeolite layer) an increase in separation factor can be expected for the binary mixtures in the combinations above – with the H_2/CO mixture showing the highest probability of achieving separation factors above the Knudsen diffusion ratios. For M2 the ideal selectivities are not convincingly higher than the corresponding Knudsen diffusion ratio, therefore it was decided to study M3 in more detail.

4.3.2 SINGLE GAS PERMEATION IN CROSS FLOW MODE

With reference to paragraph 2.4.2 *(also see Figure 2-13)*, flux or permeability in a porous membrane can be used to characterise the transport mechanism through the membrane due to observed temperature and pressure dependencies. These dependencies are graphically illustrated in Figure 4-4 a) to f) and were obtained from unary permeation experiments, conducted according to the method described in paragraph 3.2.3.

The following experiments were conducted on M3. Here a constant pressure drop (either 50 or 100 kPa) was maintained while feed pressure (P_f) and temperature (T) were varied. Figure 4-4 summarises the flux results for the gases H_2, CO_2 and CO. In a) the H_2 flux shows an overall increase in flux for the temperature ranges as the feed pressure is increased. The highest recorded flux is 0.083 mol/m^2.s at 60°C. For the temperatures 40 and 60°C the H_2 flux shows a continued increase while at 70 and 80°C a minimum is found at a feed pressure of 200 kPa. This trend is not found in b). Here the flux increases linearly for the temperatures 60 to 80°C. The change at 40°C is minimal. The highest recorded flux is achieved at 80°C and is 0.169 mol/m^2.s.

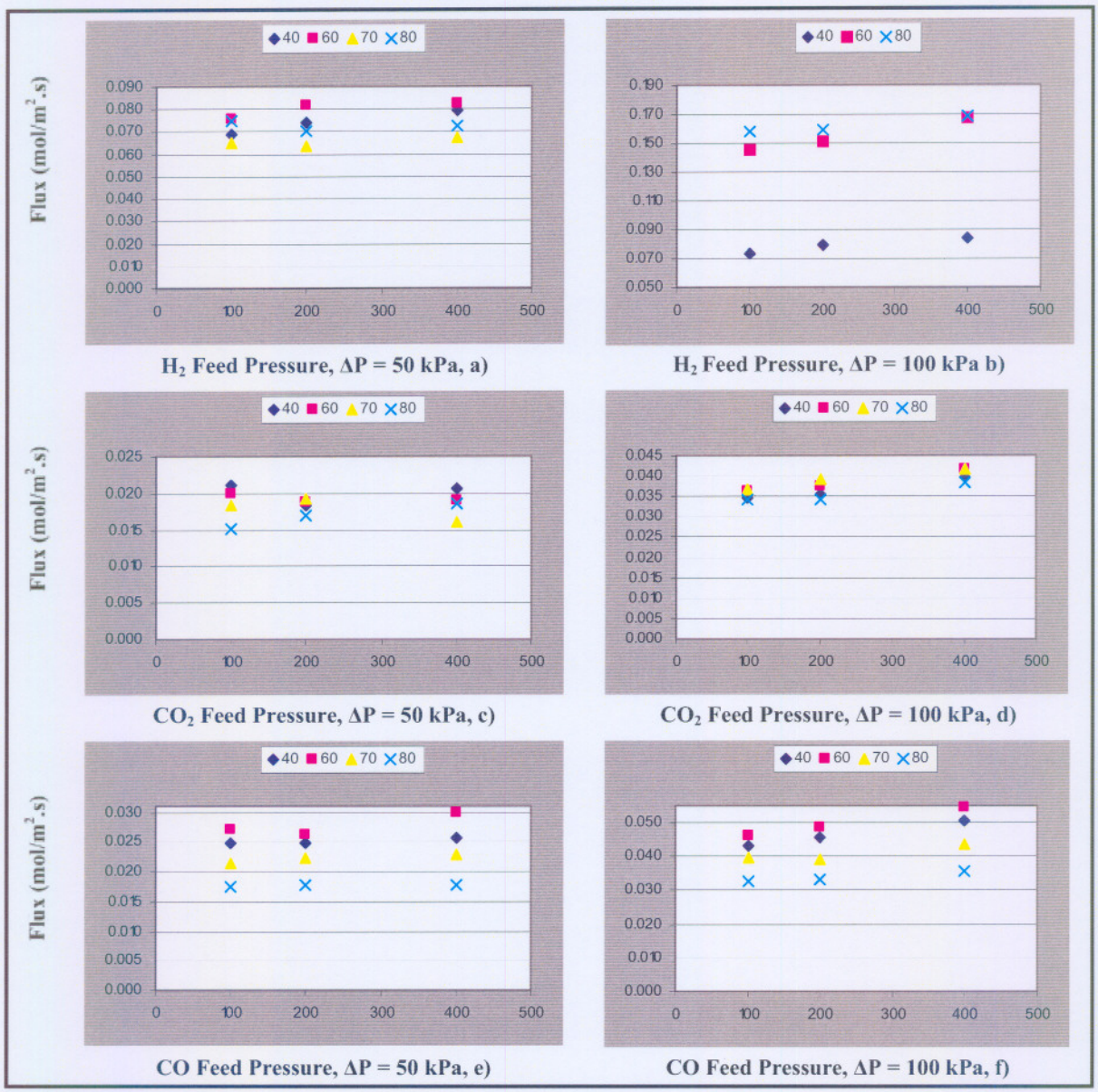

Figure 4-4: Single permeation data for H_2, CO_2 and CO through M3.

Figure c) shows the CO_2 flux at a pressure difference of 50 kPa. Here the highest flux is 0.021 mol/m^2.s which is found at a feed pressure of 100 kPa with the temperature at 40°C. This is about 25% of the flux obtained for H_2 with the same pressure drop. Similar trends are shown for the temperatures 40 and 60°C. Both have a highest flux at a pressure of 100 kPa, a minimum at 200 kPa and an incline towards 400 kPa. At 70°C the reverse is noted where the flux increase to a maximum with the pressure at 200 kPa and then falls to its lowest point at 400 kPa. The flux at 80°C show a linear increase with increasing pressure drop, similar to the trends found in d) for all the

temperature ranges. In d) the largest fluxes found are similar at 60 and 70°C with values in the region of 0.042 mol/m^2.s.

Figures 4-4 e) and f) shows the different fluxes obtained using CO. In e) an increase in flux is observed at 40 and 70°C while the flux does not change significantly at 80 °C. The flux at 60°C has a minimum at 200 kPa before going to 0.030 mol/m^2.s. This corresponds to 36% of the highest flux obtained by H_2 at a pressure difference of 50 kPa. At a pressure difference of 100 kPa the order for the highest fluxes is H_2 (0.274 mol/m^2.s) > CO (0.055 mol/m^2.s) > CO_2 (0.042 mol/m^2.s). The same general trend in temperature profile is kept in going from e) to f). At any given feed pressure the order for fluxes are 60 > 40 > 70 > 80.

By comparing graphs a) to f) it is clear that for all the cases where the pressure difference is 100 kPa the general trend in the results is more uniform. Fluxes either increase linearly or remains independent of feed pressure opposed to the maxima and minima observed in a), c) and e). This uniformity also goes for the temperature profiles. While only a single order exists for each of b), d) and f) numerous combinations are possible for a given feed pressure in a) and c).

It is also important to note the change in flux as the driving force, ΔP, is doubled from 50 to 100 kPa. For H_2 the flux also doubles at 60 and 80°C. Corresponding fluxes at 40°C remain almost unchanged. For CO_2 and CO there is a constant increase of roughly 2.0 and 1.8 respectively at all of the temperatures ranges.

Figure 4-5 shows the fluxes for the gases as a function of temperature. Note that the lines only serve as indication. In a) the temperature dependence of H_2 shows a maximum at 60°C and minimum at 70°C although the values does not change significantly over the temperature range. In b) however the flux seems to level out from 60°C.

No uniform trend can be identified in c). There exist a maximum at 200 kPa and 70°C and a minimum at 400 kPa for the same temperature. In d) a more apparent trend appears where there is a general increase in flux up to 70°C before the decline back to

80°C. This corresponds somewhat to the trend in b) where there exists a maximum at 70°C.

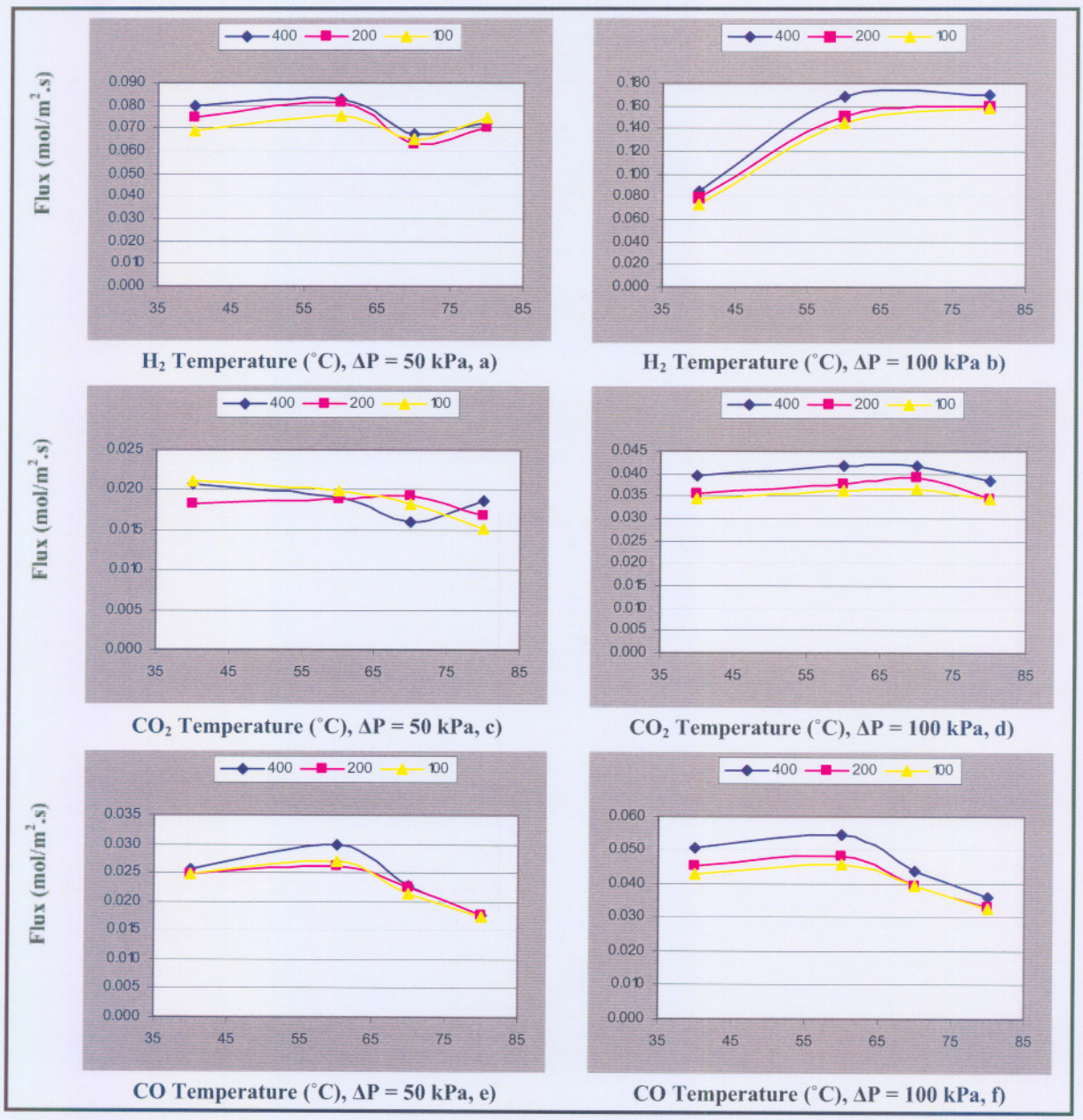

Figure 4-5: Flux as a function of temperature for M2

In e) there is again a similarity in the trends of the different feed pressures. Here the maximum is found at 60°C like in a), but no minimum is achieved. There is also no

consistency in the order of fluxes with regard to feed pressure. In f) the maximum is also found at 60°C as in e) and the order of the fluxes remain constant.

Comparing Figure 4-4 and Figure 4-5 it can again be seen that the trends in the cases where the pressure difference is 100 kPa are more uniform compared to those presented for a pressure difference of 50 kPa. This similarity is expected since both figures essentially contain the same information.

In order to evaluate/determine the transport mechanism that governs movement of molecules through M3 based on the discussion in paragraph 2.4.2 *(see Figure 2-13)*, a figure of permeability against feed pressure is needed. From eq. 2.8 – 2.16 and the discussion in paragraph 2.4.3, the pressure at the support/membrane interface must be calculated in order to determine the correct trans membrane pressure difference over the zeolite.

In order to accurately determine the correct pressure drop across the membrane, the pressure drop, and more importantly the correct transport mechanism, across the support must be determined. A first step in determining the transport mechanism is to determine the Knudsen number from eq. 2.8 for the given support. The support characteristics are given in Table 4-1. Dead-end experiments were conducted on the support using H_2 and SF_6 at 25°C with a pressure difference of 50 kPa as basis for determining the Knudsen number as they represent the extreme fluxes. The results are summarised below:

Table 4-4: KN for H_2 and SF_6 permeation through support

Parameter	Value/Range		Unit
	H_2	SF_6	
d_p	105		nm
η_i	9.21×10^{-6} N1	1.59×10^{-5} N1	Pa.s
T	298		K
$M_{w,i}$	2×10^{-3}	146×10^{-3}	kg/mol
K_N	**1.82**	**0.37**	

N1 (Determined by Aspen using RK Saove as property method)

From the results it is clear that Kn is not significantly smaller than 1 and that both Knudsen diffusion and viscous flow needs to be considered important transport

mechanisms through the support. This can *also be predicted* from literature as shown in Figure 2-12.

Taking parallel contributions from Knudsen diffusion and viscous flow [10, 42] into account, the average contributions of the two mechanisms with regard to the overall pressure drop can be determined. The exact calculations are shown and discussed in Appendix B. The results are show in Table 4-5 and Table 4-6.

Table 4-5: Values for the contribution of Knudsen diffusion, viscous flow and the membrane towards the overall of 50 kPa

Gas	Temp (°C)	Pres (kPa)	Contributions		
			Knudsen	Viscous	Membrane
H_2	40	400	0.38	0.11	0.51
	40	200	0.43	0.07	0.50
	40	100	0.44	0.05	0.51
	60	400	0.42	0.11	0.47
	60	200	0.50	0.08	0.43
	60	100	0.51	0.05	0.44
	70	400	0.35	0.09	0.56
	70	200	0.39	0.06	0.55
	70	100	0.45	0.04	0.51
	80	400	0.39	0.10	0.51
	80	200	0.45	0.07	0.49
	80	100	0.52	0.05	0.43
CO_2	40	400	0.24	0.19	0.57
	40	200	0.32	0.14	0.54
	40	100	0.46	0.14	0.41
	60	400	0.24	0.18	0.58
	60	200	0.35	0.15	0.50
	60	100	0.47	0.13	0.41
	70	400	0.22	0.15	0.64
	70	200	0.38	0.15	0.47
	70	100	0.44	0.12	0.44
	80	400	0.26	0.17	0.56
	80	200	0.34	0.13	0.52
	80	100	0.38	0.10	0.53
CO	40	400	0.32	0.17	0.51
	40	200	0.42	0.13	0.45
	40	100	0.50	0.10	0.40
	60	400	0.40	0.20	0.40
	60	200	0.48	0.14	0.38
	60	100	0.58	0.11	0.31
	70	400	0.32	0.15	0.53
	70	200	0.42	0.12	0.46
	70	100	0.47	0.09	0.45
	80	400	0.26	0.12	0.62
	80	200	0.34	0.09	0.57
	80	100	0.39	0.07	0.54

Table 4-6: Values for the contribution of Knudsen diffusion, viscous flow and the membrane towards the overall pressure drop of 100 kPa

Gas	Temp (°C)	Pres (kPa)	Contributions		
			Knudsen	Viscous	Membrane
H_2	40	400	0.20	0.06	0.74
	40	200	0.23	0.04	0.73
	40	100	0.23	0.03	0.74
	60	400	0.43	0.11	0.46
	60	200	0.46	0.07	0.47
	60	100	0.48	0.05	0.47
	70	400	0.72	0.18	0.10
	70	200	0.78	0.12	0.10
	70	100	0.83	0.08	0.09
	80	400	0.45	0.11	0.43
	80	200	0.51	0.07	0.42
	80	100	0.55	0.05	0.40
CO_2	40	400	0.23	0.18	0.59
	40	200	0.30	0.14	0.55
	40	100	0.38	0.11	0.51
	60	400	0.27	0.19	0.54
	60	200	0.35	0.15	0.50
	60	100	0.43	0.12	0.46
	70	400	0.28	0.19	0.52
	70	200	0.38	0.15	0.46
	70	100	0.44	0.12	0.44
	80	400	0.27	0.18	0.55
	80	200	0.35	0.13	0.52
	80	100	0.43	0.11	0.47
CO	40	400	0.32	0.17	0.52
	40	200	0.39	0.12	0.49
	40	100	0.43	0.09	0.48
	60	400	0.37	0.18	0.45
	60	200	0.44	0.13	0.43
	60	100	0.49	0.09	0.41
	70	400	0.31	0.15	0.55
	70	200	0.37	0.10	0.53
	70	100	0.43	0.08	0.49
	80	400	0.26	0.12	0.62
	80	200	0.32	0.09	0.59
	80	100	0.37	0.06	0.57

From the table it is evident that the influence of Knudsen diffusion is the most prominent resistance to transport in the support. The influence of the membrane itself to the overall pressure drop is about 49% on average, while the rest is as a result of

the pressure drop across the support. The influence of Knudsen diffusion increases as the absolute pressure drop is decreased, while viscous flow is directly proportional to an increase in pressure drop. This is expected since viscous flow is next to its dependence on pressure drop, also dependent on the absolute pressure.

Another observation from Table 4-5 is that the resistance to transport in the support layer is significant, with resistances being as high as 55%. This was also concluded by Zah [6] for pervaporation, where resistances in the support were determined to be in the order of 60%. Using this information the actual pressure difference over the zeolite and the subsequent permeability's can now be calculated and are given in Figure 4-6 - Figure 4-8.

Knowing the pressure drop over the zeolite layer, permeability can now be calculated from the experimental results, which are presented in Figure 4-6 to Figure 4-8 below. Figure 4-6 represents the permeability of H_2 for the different temperatures and pressures discussed. The highest permeability value (for pressure differences of 50 kPa) of 3.81 x 10^{-6} mol/m^2.s.Pa is found at a feed pressure of 200 kPa and 60°C. The lowest recorded permeability (for the same pressure difference) is 2.31 x 10^{-6} mol/m^2.s.Pa. In b) the highest permeability was 4.01 x 10^{-6} mol/m^2.s.Pa. Zhu *et al.* [17] found permeation rates in the order of 2.5 – 3.0 x 10^{-7} mol/m^2.s.Pa, while Xu *et al.* [13 - 15] published permeation rates of 2.86 x 10^{-7} mol/m^2.s.Pa for H_2 at 40°C and a feed pressure of roughly 100 kPa. At similar conditions for M3 the permeability was calculated as 9.89 x 10^{-7} mol/m^2.s.Pa. This is approximately 3 times higher than that found by [15] and [17]. A final remark is the fact that the permeability values in both a) and b) tend to remain constant as the feed pressure is varied.

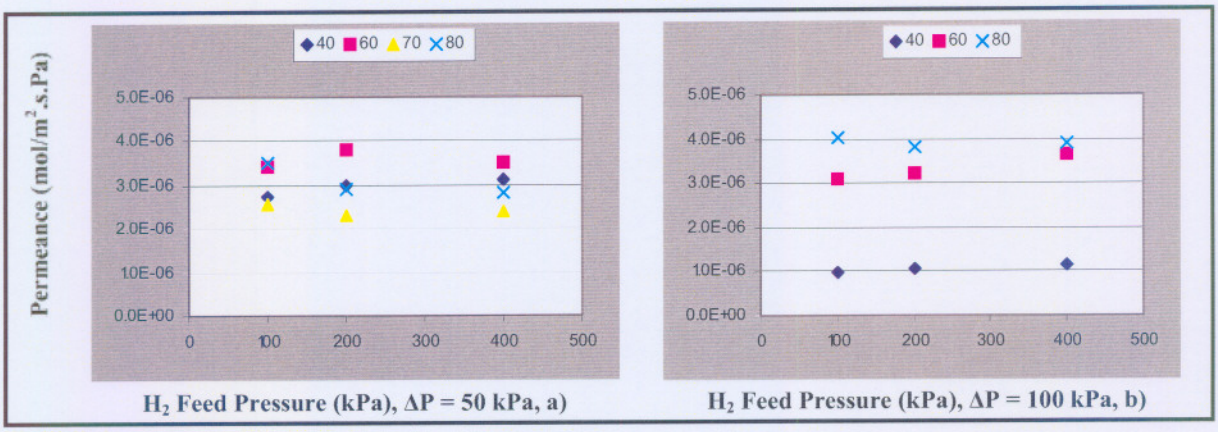

Figure 4-6: Pressure and temperature dependencies of the permeability of H_2

The experimental figures for CO_2 are presented in Figure 4-7. In a) no common trend can be observed for the different permeability's. The maximum permeability of 1.04 x 10^{-6} mol/m^2.s.Pa occurs when the temperature is at 40°C and the feed pressure is 100 kPa. Permeability values are of the same order in going from a) to b), although Figure 4-7 b) shows that the permeability values does not change significantly as the feed pressure is varied. The maximum permeability of 8.51 x 10^{-7} mol/m^2.s.Pa is found at 200 kPa and 70°C. This permeability is of the same order as the 2.19 x 10^{-7} mol/m^2.s.Pa found by [16] for CO_2 in a silicalite-1 membrane on a α-alumina disk at 25°C and a pressure difference of 80 kPa.

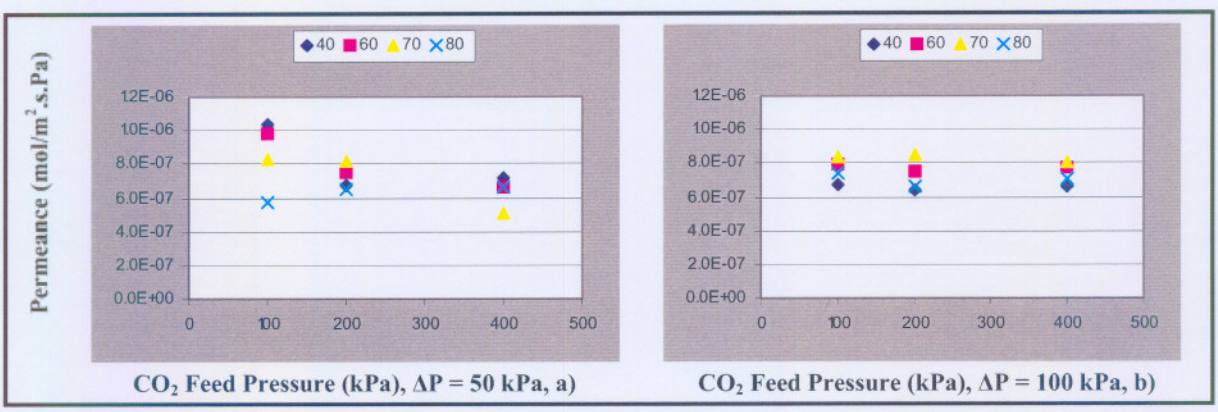

Figure 4-7: Pressure and temperature dependencies of the permeability of CO_2

In Figure 4-8 a) the permeability dependencies for CO can be seen as a function of feed pressure. The highest permeability recorded here is 1.51 x 10^{-6} mol/m^2.s.Pa. On

average, these values do not vary significantly as the feed pressure is varied. This trend is also seen in Figure 4-8 b). The highest permeability calculated here is 1.22 x 10^{-6} mol/m^2.s.Pa. Zhu [17] found a unary permeation rate for CO of about 1.00 x 10^{-7} mol/m^2.s.Pa. A value of 8.98 x 10^{-7} mol/m^2.s.Pa was found for CO at similar conditions in this study.

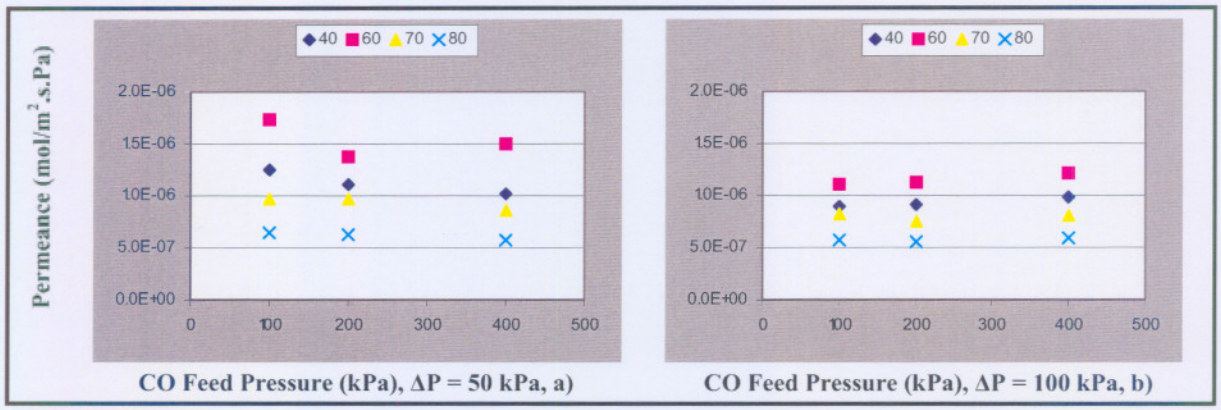

Figure 4-8: Pressure and temperature dependencies of the permeability of CO

From the discussion regarding flux and permeability above certain conclusions can be drawn regarding transport in M3. Transport according to viscous flow is the only mechanism that results in an increase in permeability as the feed pressure increases. As this is not the case in either of Figure 4-6, Figure 4-7 or Figure 4-8 it can be concluded that viscous flow is absent, which is expected for microporous membranes. The dependence of permeability as a function of the absolute pressure drop is an important characteristic of membrane quality. The permeability resulting from Knudsen diffusion is independent of pressure drop corresponding to a linear relationship between the flux and pressure drop. This is the case for the corresponding permeability and flux for H_2, CO and CO_2 at a pressure drop of 100 kPa as shown by Figure 4-4 b), d) and f) and Figure 4-6 b), Figure 4-7 b) and Figure 4-8 b). From this the conclusion can be drawn that Knudsen diffusion is the governing transport mechanism for H_2, CO_2 and CO through the NaA layer.

4.4 BINARY GAS PERMEATION THROUGH A SUPPORTED ZEOLITE MEMBRANE

4.4.1 INTRODUCTION

Binary permeation experiments were carried out at 40 °C, with ΔP = 100 kPa. Three sets of experiments were carried out, one for each gas mixture; H_2/CO_2, H_2/CO and CO/CO_2. For each set of experiments three variables were investigated; the feed pressure (P), the feed flow rate ($\phi_{v,F}$), and the feed composition (y_i). The experimental sequence for a given binary mixture *(see paragraph 3.2.3 for experimental configuration)* is given below:

Table 4-7: Experimental sequence for binary experiments

Sequence	Flow rate (ml/min)	Feed pressure kPa	Composition -
1	320	100	0.8/0.2
	320	200	0.8/0.2
	320	400	0.8/0.2
2	320	100	0.5/0.5
	320	200	0.5/0.5
	320	400	0.5/0.5
3	320	100	0.2/0.8
	320	200	0.2/0.8
	320	400	0.2/0.8
4	500	100	0.5/0.5
	500	200	0.5/0.5
	500	400	0.5/0.5

In order to calculate the correct permeability for the binary mixture the effect of the support influence (as calculated by the single permeation data) was incorporated into the calculation (shown in Appendix B). Table 4-8 shows the values that were used to account for the influence of resistances in the support used in eq. 2.15.

Table 4-8: Average values for the contribution of Knudsen diffusion, viscous flow and the membrane towards the overall pressure drop for ΔP = 100 kPa and T = 40°C

Component	Pressure (kPa)	Contributions		
		Knudsen	Viscous	Membrane
H_2	400	0.20	0.06	0.74
	200	0.23	0.04	0.73
	100	0.23	0.03	0.74
CO_2	400	0.23	0.18	0.59
	200	0.30	0.14	0.55
	100	0.28	0.11	0.51
CO	400	0.32	0.17	0.52
	200	0.39	0.12	0.49
	100	0.43	0.09	0.48

4.4.2 CO-CO_2 MIXTURES

In Figure 4-9 below the permeation data for a binary mixture of CO and CO_2 are presented. For comparison, the single component permeability's are included. a) shows the permeability for an 80% mixture of CO. In this case the permeate rate of CO is nearly a factor 0.7 of that for unary permeability at the same conditions. The CO_2 permeability however is virtually equal to the corresponding unary permeability. This is also the case for other compositions like that presented in b) and c). From this it is clear that the permeability of CO_2 is not affected by the presence of CO. Also, that the permeability of CO decreases in a mixture containing CO_2 compared to its unary permeability.

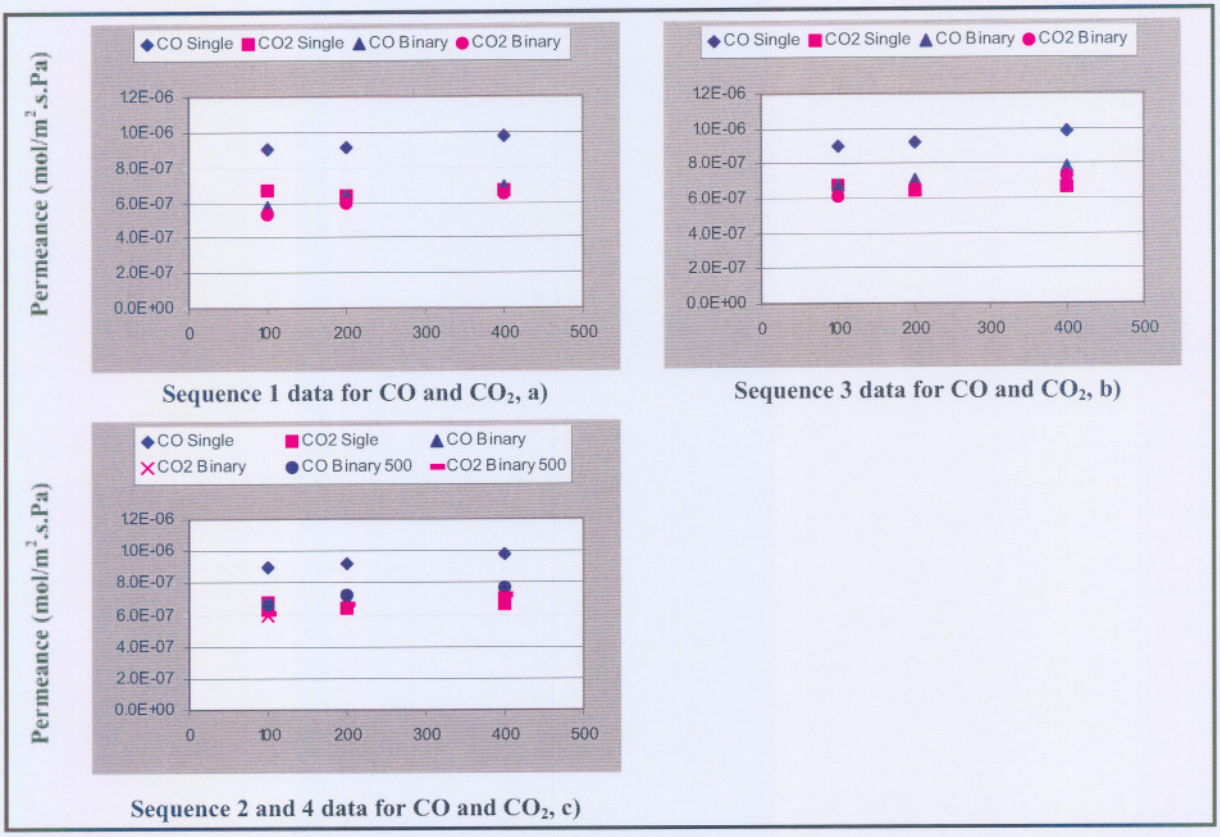

Figure 4-9: Binary permeation data for CO and CO_2 mixtures

In c) the permeability for a 50/50 mixture of CO/CO_2 at different feed flow rates is shown. From the figure it can be concluded that the feed flow rate has no effect on the selectivity of M3, which is also shown in Table 4-9 below. Furthermore, it is apparent that mixtures enter and leave M3 in the same composition that it enters and that no significant separation occurs for the given combinations of mixtures. Since only little separation is achieved, Eq. 2.1 has been used for the calculation of the separation factor.

Table 4-9: Selectivities for sequence 1 to 4

Sequence	Pressure (kPa)	$\phi_{v,CO}$ (ml/min)	$\phi_{v,CO2}$ (ml/min)	Π_{CO} (10^{-7}) mol/m^2.s.Pa	Π_{CO2} (10^{-7}) mol/m^2.s.Pa	$\alpha_{CO/CO2}$
1	400	123.3	30.7	6.92	6.48	1.01
	200	137.2	34.2	6.36	5.98	1.00
	100	149.2	37.1	5.72	5.36	1.00
2	400	36.2	140.1	7.78	7.33	1.00
	200	38.0	150.0	7.05	6.55	1.01
	100	41.9	167.9	6.71	6.12	1.03
3	400	86.5	85.0	7.50	7.01	1.01
	200	92.2	91.2	6.84	6.37	1.01
	100	101.1	100.4	6.42	5.94	1.02
4	400	88.8	87.4	7.68	7.20	1.00
	200	96.8	94.4	7.18	6.63	1.02
	100	103.5	103.1	6.59	6.10	1.02

4.4.3 CO-H_2 MIXTURES

In Figure 4-10 below the binary results for CO/H_2 mixtures are presented. In a) the permeability data of an 80% CO mixture is shown. Comparing the CO permeability in a CO_2 mixture (in Figure 4-9 a)) to that in a H_2 mixture (in Figure 4-10 a)) it can be seen that higher permeability is obtained for CO in the H_2 mixture. Here the CO permeability is about 10% higher. The permeability of both CO and H_2 is lower than their corresponding unary permeability in a). This is not the case in b). Here the permeability of both CO and H_2 is higher that their unary permeability at a feed pressure of 100 kPa. At 200 kPa the binary and unary values do not differ significantly and at 400 kPa the permeability of both species is lower than the unary permeability.

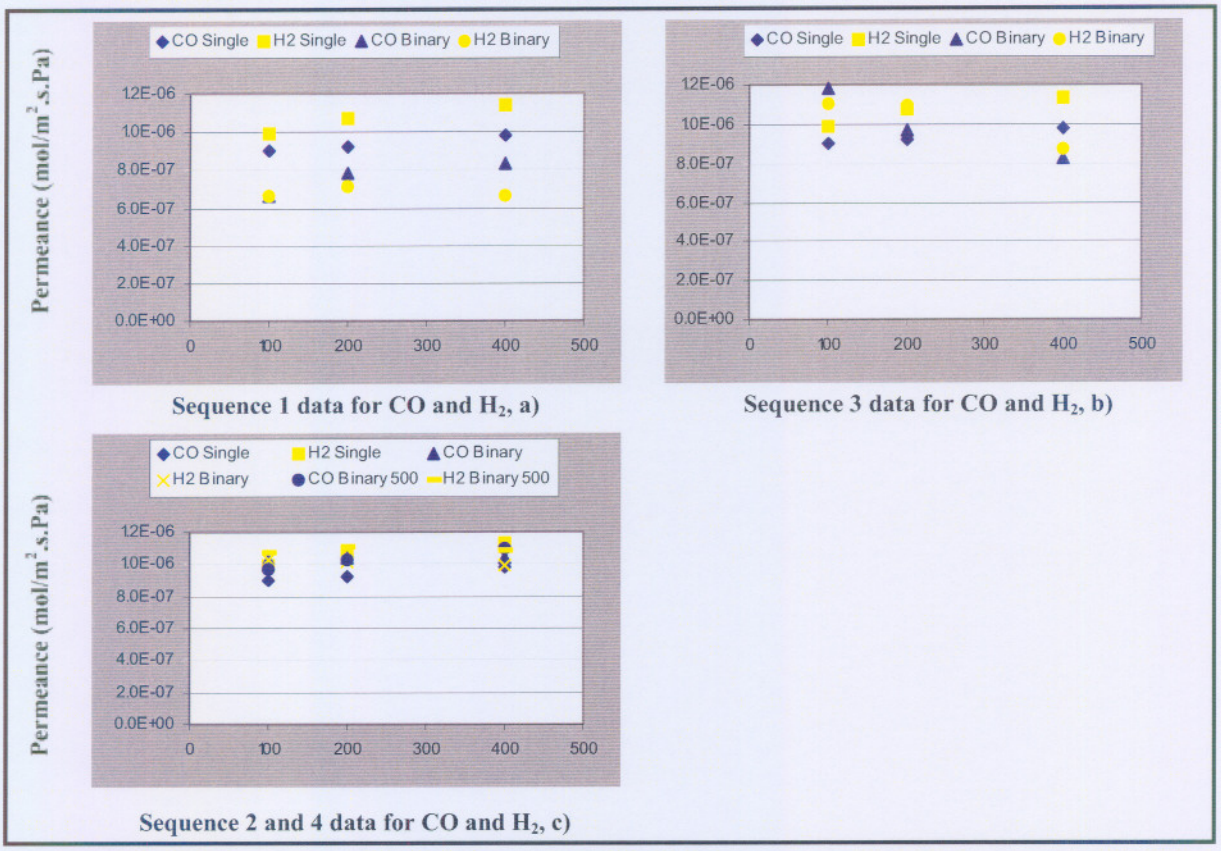

Figure 4-10: Binary permeation data for H_2 and CO mixtures

In c) the 50/50 mixtures for CO/H_2 are shown. Again, the effect of the feed flow rate does not seem to have an influence on the permeation data. In this case, the observed permeability of both CO and H_2 is similar to that of the corresponding unary permeability. Again, it can be concluded that separation factors are close to unity and that no significant separation takes place for the given mixture.

Table 4-10: Selectivities for sequence 1 to 4

Sequence	Pressure (kPa)	$\phi_{v,CO}$ (ml/min)	$\phi_{v,H2}$ (ml/min)	Π_{CO} (10^{-7}) mol/m^2.s.Pa	Π_{H2} (10^{-7}) mol/m^2.s.Pa	$\alpha_{CO/H2}$
1	400	142.8	37.8	8.30	6.61	1.18
	200	168.6	40.7	7.82	7.10	1.04
	100	179.0	37.9	6.62	6.60	0.94
2	400	63.6	252.2	8.27	8.76	0.83
	200	52.4	251.8	9.71	10.99	0.89
	100	44.6	200.7	11.80	11.01	1.01
3	400	139.1	147.4	10.44	9.97	0.99
	200	139.9	145.4	10.38	10.15	0.96
	100	140.7	142.8	10.32	10.30	0.94
4	400	130.1	153.6	10.94	10.83	0.95
	200	139.0	159.1	10.31	11.12	0.87
	100	147.4	155.1	9.66	10.72	0.85

4.4.4 CO_2-H_2 MIXTURES

In Figure 4-11 only the permeation results for a 50/50 mixture of CO_2 and H_2 is presented. Since no separation was obtained for CO (highest adsorption affinity) and H_2 (lowest affinity) it was expected that no separation will take place for this mixture. Figure 4-11 and Table 4-11 confirms this expectation, as the selectivity of the species tend to unity.

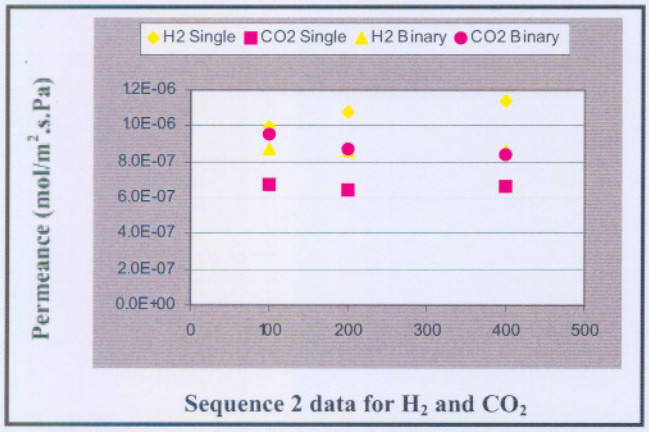

Figure 4-11: Binary permeation data for H_2 and CO_2 mixtures

It can be seen that CO_2 has higher permeability values in the binary mixture with H_2 than its corresponding unary permeability.

Table 4-11: Selectivities for sequence 2

Sequence	Pressure (kPa)	$\phi_{v,CO2}$ (ml/min)	$\phi_{v,H2}$ (ml/min)	Π_{CO2} (10^{-7}) mol/m^2.s.Pa	Π_{H2} (10^{-7}) mol/m^2.s.Pa	$\alpha_{CO2/H2}$
2	**400**	135.6	116.9	8.33	8.55	1.16
	200	124.0	115.6	8.66	8.58	1.07
	100	119.3	115.2	9.47	8.68	1.04

Following the results obtained from paragraph 4.4 it can be concluded that the studied M3 is not suited for separating gas mixtures containing H_2, CO and CO_2. Since the adsorption affinity of the gasses to NaA increases in going from H_2 to CO_2 to CO it was expected that species like CO and CO_2 might block the movement of the component with the lower affinity at the low temperatures using in this study. Zhu [17] showed this for water permeation. Another factor that should be taken into consideration is the effect of intercrystalline diffusion. Figure 4-3 shows the microscopic surface of M3, and this surface is typical for a NaA membrane sintered for 3.5 hours, which was the sintering time that gave excellent results for pervaporation of water from alcohol/water mixtures [6]. However in a later study by van Niekerk [37]. It was shown that a zeolite with a sintering time of at least 4.0 hrs is suitable closed for gas separation, which was demonstrated with the separation of n-butane from isobutane, showing selectivities up to 500. From this, it can be concluded that the sintering time of 3.5 hours was not sufficient to form a gas selective membrane, since intercrystalline diffusion will dominate the transport rate.

CHAPTER 5: CONCLUSIONS AND RECOMMENDATIONS

5.1.1 CONCLUSIONS

For this study, centrifugally casted tubular alumina supports, prepared from AKP-30 powder, were used as support in the synthesis of two composite NaA membranes; M2 prepared with a double layer and M3 that was made with three coatings. As concluded from Scanning Electron Microscopy a crystal layer of approximately 10 μm was formed with the triple synthesis extensively covering the support surface. Although good coverage, it was also obtained that the crystals-growth was not finished completely at a synthesis time of 3.5 hour.

From single gas experiments it was found that M3 showed an improved ideal selectivity, but a lower permeability than M2, and because of the better selectivity, M3 was studied in more detail.

The ideal separation factors for M3 were in the region of the Knudsen selectivity. An explanation for the relative low separation factors was the occurrence of intercrystalline diffusion, which was confirmed by the permeation of SF_6. Pressure and temperature did not have a significant effect on the ideal selectivity.

With respect to the mass transfer across the membrane, it was found that Knudsen diffusion in the support dominated in H_2 transport and contributed to between 42% and 50% of the resistance across the membrane. The contribution of viscous flow in the support ranged between 5% and 11%. For CO_2 the effect of Knudsen diffusion was lower, ranging from 25% to 43%, while viscous flow was higher at 12% to 14%. In the case of CO Knudsen diffusion was from 32% to 46% and viscous flow from 9% to 16%.

By taking Knudsen diffusion and viscous flow parallel, the permeability of H_2, CO and CO_2 through the zeolite layer was determined. For H_2 the highest permeability of 3.81 x 10^{-6} mol/m^2.s.Pa was found at a pressure difference of 50 kPa, which was a factor 3 higher than similar values reported in literature. For CO_2 the highest permeability was 1.04 x 10^{-6} mol/m^2.s.Pa for a pressure difference of 50 kPa at 40°C, while the lowest permeability of 8.51 x 10^{-7} mol/m^2.s.Pa was found at 100 kPa also at 40°C. In the case of CO, a permeability of 8.98 x 10^{-7} mol/m^2.s.Pa was found at a pressure difference of 100 kPa and 40°C, which was similar to literature values obtained under similar conditions.

Finally, experiments with binary mixtures of H_2, CO and CO_2 were conducted. In these experiments, it was shown that the feed flow rate has no effect on the permeation of different components through the membrane. It was also shown that the NaA membrane showed no significant selectivity towards any of the components and as result separation factors were in the order of unity. From this it can be concluded that the prepared NaA membrane used is not suitable for separating mixtures of H_2, CO and CO_2.

5.1.2 RECOMMENDATIONS

Although identical prepared NaA zeolites showed good results for pervaporation of water, it did not give promising results in the separation of H_2, CO and CO_2. One reason for the poor selectivity could be the relative short synthesis time. A synthesis time of 4 hours could give improved selectivity's and is therefore recommended.
If results with a prolonged synthesis time do not give an improved selectivity, it would be suggested to use another type of zeolite, *e.g.* silicalite, which due to its hydrophobic character will prohibit the occurrence of intercrystalline diffusion.

CHAPTER 6: REFERENCES

[1] IEA Publications. 1998. Future role of coal. [Available on internet] http://cdnet.stic.gov.tw/ebooks/OECD/57.pdf

[2] IEA. 2003. Findings of recent IEA work 2003. [Available on internet] http://www.iea.org/dbtw-wpd/bookshop/add.aspx?id=126

[3] IEA. 2003. Prospects for hydrogen from coal. [Available on internet] http://www.iea-coal.org.uk

[4] EC. 2003. Hydrogen energy and fuel cells – a vision of our future. High level group on hydrogen and fuel cells. [Available on internet] http://europa.eu.int/comm/research/energy/pdf/hlg_interim_report_en.pdf

[5] H.H. Funke, M.G. Kovalchick, J.L. Falconer, and R.D. Noble, 1996, Separation of hydrocarbon isomer vapours with silicalite zeolite membranes, Ind. Eng. Chem. Res., **35**, 1575

[6] J. Zah, H.M. Krieg, H.W.J.P. Neomagus & J.C. Breytenbach. Synthesis optimisation of zeolite A membranes on centrifugally casted ceramic supports. Presented at ICOM 2005, Seoul, South Korea.

[7] Hsieh, H.P. 1996. Inorganic membranes for separation and reaction. 1st ed. Amsterdam: Elsevier Scientific Publishing Company. p. 1-591.

[8] Mulder, M. 1996. Basic principles of membrane technology. 2nd ed. Dordrecht : Kluwer Academic Publishers. p. 168-172

[9] Meares, P. 1976. Membrane separation processes. 1st ed. Amsterdam: Elsevier Scientific Publishing Company. p. 2-4.

[10] Van de Graaf, J.M., 1999, Permeation and separation of supported silicalite-1 membranes. A modeling approach, PhD thesis, university Delft

[11] McCusker, L.B. & Baerlocher, C. 2001. Zeolite Structures. (*In* Van Bekkum, H., Flanigen, E.M., Jacobs, P.A. & Jansen, J.C., eds. Introduction to zeolite science and practice. Amsterdam, The Netherlands : Elsevier. P. 37-67.)

[12] C. Baerlocher, W. M. Meier, & D. H. Olson, 2000, Atlas of zeolite framework types, Elsevier, Amsterdam, The Netherlands, 5th ed.

[13] X. Xu, W. Yang, J. Lui & L. Lin, 2001, Synthesis of NaA zeolite membranes from clear solution, Microporous and Mesoporous Materials, **43**, 299-311

[14] X. Xu, W. Yang, J. Lui & L. Lin, 2001, Synthesis and perfection evaluation of NaA zeolite membrane, Separation and Purification Technology, **25**, 475-485

[15] X. Xu, Y. Bao, C. Song, W. Yang, J. Lui & L. Lin, 2005, Synthesis, characterisation and single gas permeation properties of NaA zeolite membrane, J. Membrane Sciences, **249**, 51-64

[16] C. Algieri, P. Bernardo, G. Golemme, G. Barbieri & E. Drioli, 2003, Permeation properties of a thin silicalite-1 (MFI) membrane, J. of Membrane Sciences, **222**, 181-190

[17] W. Zhu, L. Gora, A.W.C van den Berg, F. Kapteijn, J.C. Jansen & J.A. Moulijn, 2005, Water vapour separation from permanent gases by a zeolite-4A membrane, J. Membrane Sciences, **253**, 57-66

[18] W.J.W. Bakker, L.J.P. van den Broeke, F. Kapteijn, & J.A. Moulijn, 1997, Temperature dependance of one-component permeation through a silicalite-1 membrane, AIChE J., **43**, 2203-2214

[19] L.J.P. van den Broeke, W.J.W. Bakker, F. Kapteijn & J.A. Moulijn, 1999, Transport and separation properties of a silicalite-1 membrane – I. Operating conditions, Chemical Engineering Science, **54**, 245-258

[20] W.J.W. Bakker, F. Kapteijn, J. Poppe & J.A. Moulijn, 1996, Permeation characteristics of a metal-supported silicalite-1 zeolite membrane, J. of Membrane Sciences, **117**, 57-78

[21] F. Kapteijn, J. van de Graaf & J.A. Moulijn, 1998, The Delft silicalite-1 membrane: peculiar permeation and counter-intuitive separation phenomena, J. Molecular Catalysts, **134**, 201-208

[22] L.J.P. van den Broeke, F. Kapteijn & J.A. Moulijn, 1999, Transport and separation properties of a silicalite-1 membrane – II. Variable separation factor, Chemical Engineering Science, **54**, 259-269

[23] J.M. van de Graaf, E. van der Bijl, A. Stol, F. Kapteijn & J.A. Moulin, 1998, Effect of operating conditions and membrane quality on the separation performance of composite silicalite-1 membranes, Ind. Eng. Chem. Res., **37**, 4071-4083

[24] C. Bai, M. Jai, J.L. Falconer & R.D. Noble, 1995, Preparation and separation properties of silicalite composite membranes, J. Membrane Sciences, **105**, 79-87

[25] P. Ciavarella, H. Moueddeb, S. Miachon, K. Fiaty & J. Dalmon, 2000, Experimental study and numerical simulation of hydrogen/isobutene permeation and separation using MFI-zeolite membrane reactor, Catalyst Today, **56**, 253-264

[26] E.R. Geus, M.J. den Exter & H. van Bekkum, 1992, Synthesis and characterization of zeolite (MFI) membranes on porous ceramic supports, J. Chem. Soc. Faraday Trans., **88**(20), 3101-3109

[27] J. Hedlund, M. Noack, P. Kölsch, D. Creaser, J. Caro & J. Sterte, 1999, ZSM-5 membrane synthesized without organic templates using a seeding technique, J. Membrane Sciences, **159**, 263-273

[28] Y. Hasegawa, K. Watanabe, K. Kasukabe & S. Morooka, 2001, The separation of CO_2 using Y-type zeolite membranes ion-exchanged with alkali metal cations, Separation and Purification Technology, **22-23**, 319-325

[29] N. Nishiyama, K. Ueyama & M. Matsukata, 1997, Gas permeation through zeolite-alumina composite membranes, AIChE J., **43**, 2724- 2728

[30] T. Tomita, K. Nakayama & H. Sakai, 2004, Gas separation characteristics of DDR type zeolite membrane, Microporous and Mesoporous Materials, **68**, 71-75

[31] R. M. Barrer, 1990, Porous crystal membranes, J. Chem. Soc. Faraday Trans., **86**, 1123-1130

[32] P.B. Weisz, CHEMTECH 3 (1973) 498

[33] M. Hanebuth, R. Dittmeyer, G.T.P Mabande & W. Schwieger. 2005. On the combination of different transport mechanisms for the simulation of steady-state mass transfer through stainless steel supported silicalite-1 membranes as a model system, Catalysis Today, **104**, 352-359

[34] P.M. Biesheuvel, A. Nijmeijer & H. Verweij, 1998, Theory of batchwise centrifugal casting, AIChE Journal, **44**, 1914-1920

[35] G.C. Steenkamp, 2000, Centrifugal casting and coating of tubular ceramic membrane supports, Masters dissertation, PU for CHE

[36] H. Bisset, 2005, Manufacture and optimization of tubular ceramic membrane supports, Masters dissertation, North-West University

[37] A. Van Niekerk, 2006, Direct Crystallisation of hydroxysodalite and MFI membranes on a-alumina supports, Masters dissertation, North-West University

[38] G. Xomeritakis, A. Gouzinis, S. Nair, T. Okubo & M. He. 1999. Growth, microstructure, and permeation properties of supported zeolite (MFI) films and membranes prepared by secondary growth, Chemical Engineering Science, **54**, 3521-3531

[39] G. Bonilla, M. Tsapatsis, D.G. Vlachos & G. Xomeritakis. 2001. Fluorescence confocal optical microscopy imaging of the grain boundary structure of zeolite MFI membranes made by secondary (seeded) growth, J. Membrane Sciences, **182**, 103-109

[40] L.T.Y. Au & K.L. Yeung. 2001. An investigation of the relationship between microstructure and permeation properties of ZSM-5 membranes, J. Membrane Sciences, **194**, 33-55

[41] P.H. Nelson, M. Tsapatsis & S.M. Auerbach. 2001. Modeling permeation through anisotropic zeolite membranes with nanoscopic defects, J. Membrane Sciences, **184**, 254-255

[42] E.A. Mason and A.P. Malinauskas. 1983. Gas transport in porous media: The dusty gas model. Elsevier: Amsterdam.

APPENDIX A: MFC CALIBRATION

Mass flow controllers *(Brooks Instrument, Model 5850 TR)* were used to accurately control the required flow rates and mixture compositions. In order to assure repeatability of experimentation these MFC's were calibrated at the beginning of every month. The calibration procedure was a simple procedure where a particular controller (depending on the service; H_2, CO and CO_2) was set to a certain output (0 – 100%) and the resulting flow was measured with a soap flow meter. From this data, Figures A-1 to A-3 were plotted. Valve positions could then be determined for various flow rates.

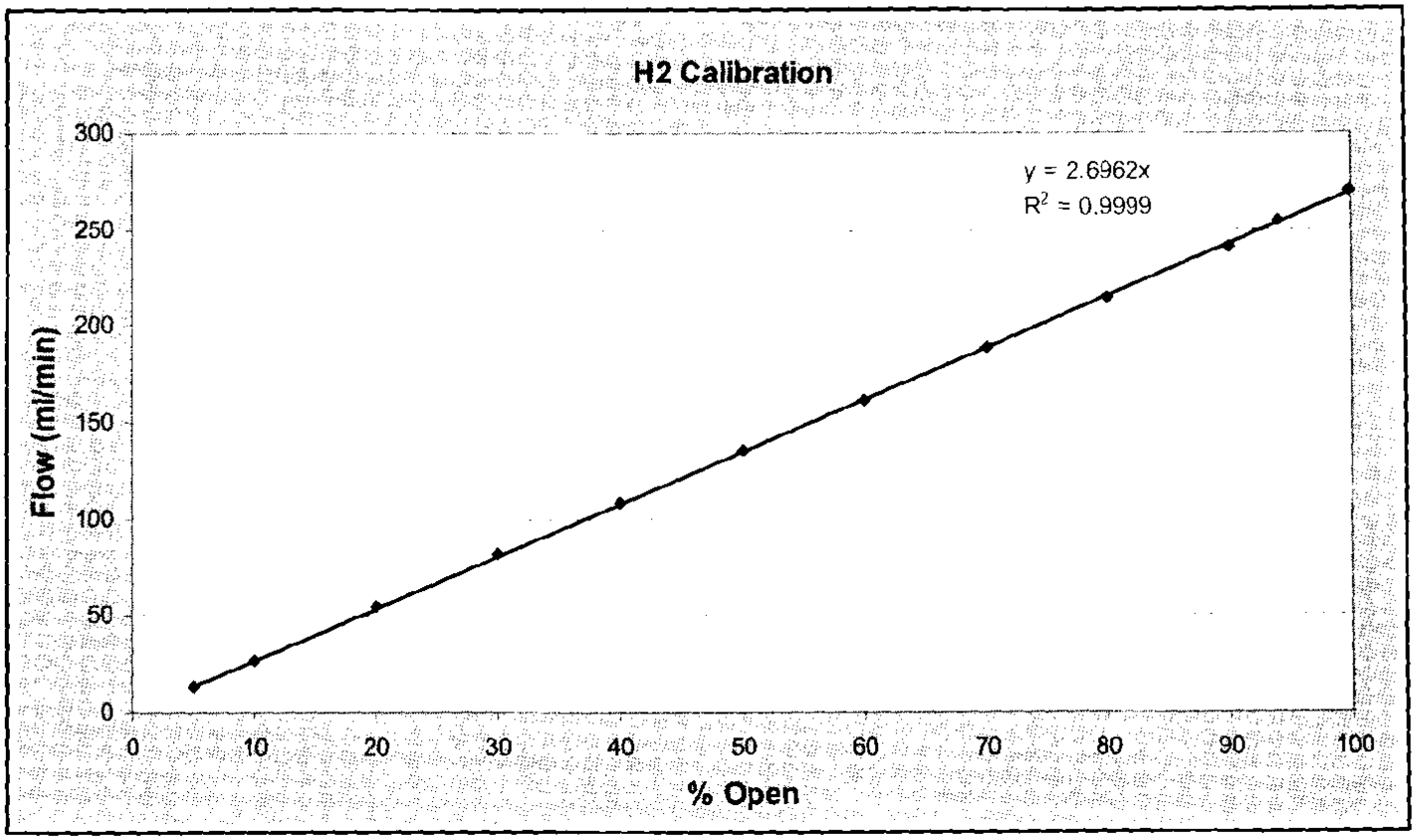

Figure A - 1: Calibration curve for H_2

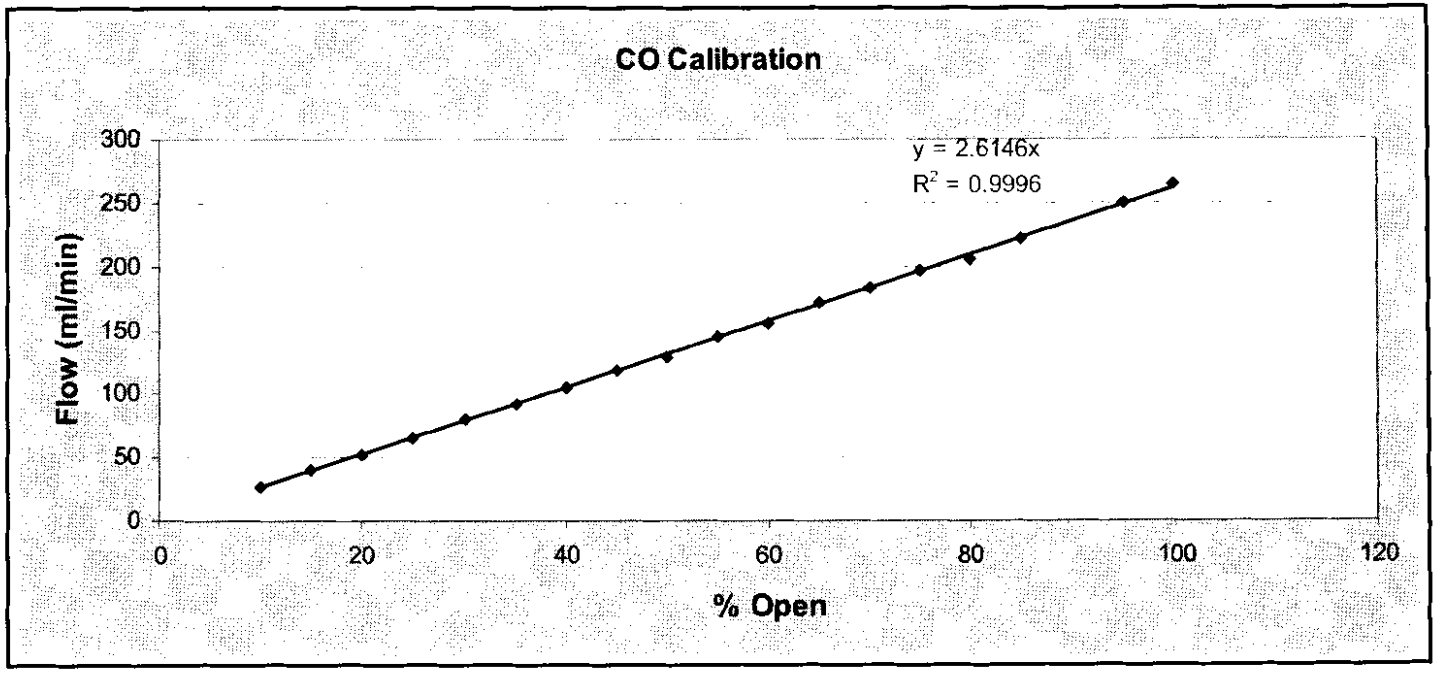

Figure A - 2: Calibration curve for CO

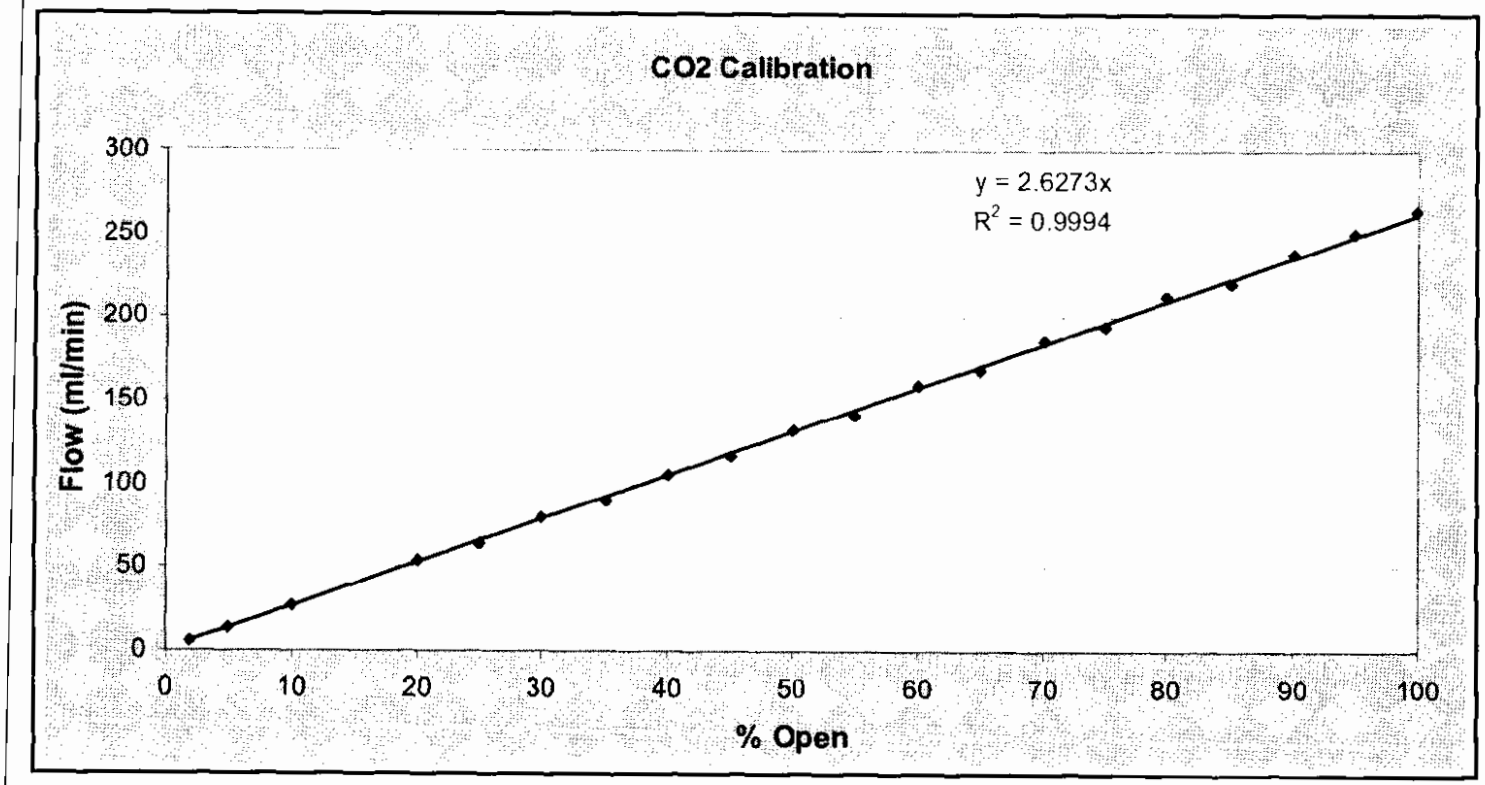

Figure A - 3: Calibration curve for CO_2

APPENDIX B: EXPERIMENTAL RESULTS

The experimental results are given in the Appendix below. Table B-1 contains the single permeation data for H_2, Table B-2 the results for CO_2 and B-3 the results for CO. The results for the binary mixtures are given in Tables B-4 to B-6. For Tables B-1 to B-3 the first 4 columns contain the experimental data. Table B-1, row 1 will be used as basis for sample calculations.

In column 5 D_{Kn} is determined from eq. 2.10.

$$D_{Kn} = \frac{2}{3}.(0.396^2).(5.24x10^{-8}).\sqrt{\frac{8.(8.3144).(40+273.15)}{(3.142).(2.02x10^{-3})}} = 9.92x10^{-6}\ \mathrm{m^2/s}$$

Column 6 contains the measured experimental flow rate ϕ_v. This is converted to flux in the next column using eq. 3.1 and 3.2. Columns 8 and 9 contain the theoretically determined values for the pressure drop resulting from Knudsen diffusion and viscous flow using eq. 2.12 and 2.14 respectively.

$$\Delta P^{Kn} = \frac{(0.0796).(8.3144).(40+273.15).(0.01039-0.00889)}{9.92x10^{-6}} = 3.13x10^4\ \mathrm{Pa}$$

$$\Delta P^{Vis} = \frac{(0.0796).(8.3144).(40+273.15).8.(9.21x10^{-6}).(0.01039-0.00889)}{(0.396^2).(5.24x10^{-8}).\left(\frac{(400+85).1000+85.1000}{2}\right)} = 1.87x10^5$$

Column 10 is the concentration (as given in Fick's first law for diffusion) term for Knudsen diffusion while columns 11 and 12 are the concentration term for viscous flow in the different units show.

$$C_{Kn} = \frac{D_{Kn}}{R.T} = \frac{9.92x10^{-6}}{(8.3144).(40+273.15)} = 3.81x10^{-9}\ \mathrm{mol/m^2.s}$$

Similarly for viscous flow:

$$C_{vis} = \frac{1}{R.T}.\frac{\varepsilon}{\tau}.\frac{r_p^2}{8.\eta_i}\overline{P} = \frac{(0.396^2).(5.24x10^{-8}).\left(\frac{(400+85).1000+85.1000}{2}\right)}{(.3144).(40+273.15).8.(9.21x10^{-6})}$$

$$= 1.09x10^{-9}\ \text{mol/m}^2.\text{s}$$

From this it follows in 13 that the total concentration is the sum of the concentration terms calculated above. In the following two columns, the different contributions for the membrane and support are calculated from Fick's first law.

$$\Delta P_{sup} = \frac{(0.0796).(0.01039-0.00889)}{(3.81x10^{-9}+1.09x10^{-9})} = 2.44x10^4\ \text{Pa}$$

And from eq. 2.16.

$$\Delta P_{mem} = 50.1000 - 2.44x10^4 = 2.56x10^4\ \text{Pa}$$

The percentage contributions of the two transport mechanisms are expressed in columns 16 and 17, while the average contributions used in Table 4-5 are given below in bold. Finally the calculated permeability is given in the final column as calculated with eq. 2.15.

$$\Pi = \frac{0.0796}{2.56x10^4}\ \text{mol/m}^2.\text{s.Pa}$$

The binary results of the CO/CO_2 mixture are shown in Table B-4. Similarly, the results of the H_2/CO mixture are given in Table B-5, while that of the H_2/CO_2 mixture is in Table B-6. In the first 4 columns under the heading *Feed*, the height and area counts (as given by the gas chromatograph) for the species involved in the feed of the mixture are given. In the subsequent 3 columns, the experimental conditions are represented as set out in Table 4-7. The next 4 columns contains the GC data for the permeate stream. In columns 12 and 13 the flow rate of the permeate and retentate

streams are given respectively (as determined by soap flow measurements). Using eq. C1 and C2 given in Appendix C, the flow rates of the concerned species in the permeate can be determined. This is followed by the membrane selectivity (α) in column 16. In the last 4 columns, the permeability and flux of the individual components are given as discussed in paragraph 4.4.1. For this the CO/CO_2 (CO 80%) mixture in Table B-4 at a 100 kPa feed pressure is used as sample calculation.

Sample calculation for CO flow rate:

$$\phi_{v,CO} = \left(\frac{(3119/0.8 + 3138/0.8 + 3138/0.8)}{3}\right).3094.156 = 123.3 \text{ ml/min}$$

Sample calculation for CO_2 flow rate:

$$\phi_{v,CO2} = \left(\frac{(2862/0.2 + 2877/0.2 + 2893/0.2)}{3}\right).2832.156 = 30.7 \text{ ml/min}$$

Flux values are again determined from eq. 3.1 and 3.2. For permeance the flux value is divided by the partial pressure drop of the relevant gas (modified by multiplying the partial pressure with the average values for the contribution of the membrane towards the overall pressure drop for ΔP = 100 kPa and T = 40°C as given in Table 4-8).

Sample calculation for CO permeance:

$$\Pi_{CO} = \frac{2.20x10^{-2}}{(0.48).100.(0.8).1000} = 5.72x10^{-7} \text{ mol/m}^2\text{.s.Pa}$$

Sample calculation for CO_2 permeance:

$$\Pi_{CO2} = \frac{5.47x10^{-3}}{(0.51).100.(0.2).1000} = 5.36x10^{-7} \text{ mol/m}^2\text{.s.Pa}$$

Table B 1: Experimental results for single permeation experiments of H_2

T (°C)	η (Pa.s)	P (kPa)	ΔP (kPa)	D_{Kn} $m^2.s$	ϕ_v ml/min	J $mol/m^2.s$	Knudsen ΔP (Pa)	Viscous ΔP (Pa)	D_{Kn}/RT mol/m2.s	$(\varepsilon/\tau)*r2/(8*\eta)$ $m^3/m^2.s$	$mol/m^2.s$	C tot	Support ΔP (Pa)	Membrane ΔP (Pa)	Vis %	Kn %	Permeability $mol/m^2.s.Pa$
40	9.21E-06	400	50	9.92E-06	446.9	0.080	3.132E+04	1.867E+05	3.81E-09	5.84E-12	1.09E-09	4.90E-09	2.44E+04	2.56E+04	0.11	0.38	3.105E-06
40	9.21E-06	200	50	9.92E-06	418.1	0.074	2.930E+04	2.690E+05	3.81E-09	5.84E-12	6.40E-10	4.45E-09	2.51E+04	2.49E+04	0.07	0.43	2.990E-06
40	9.21E-06	100	50	9.92E-06	388.1	0.069	2.720E+04	3.422E+05	3.81E-09	5.84E-12	4.15E-10	4.23E-09	2.45E+04	2.55E+04	0.05	0.44	2.714E-06
60	9.61E-06	400	50	1.02E-05	463.3	0.083	3.349E+04	2.148E+05	3.70E-09	5.60E-12	9.81E-10	4.68E-09	2.65E+04	2.35E+04	0.11	0.42	3.507E-06
60	9.61E-06	200	50	1.02E-05	457.7	0.082	3.309E+04	3.269E+05	3.70E-09	5.60E-12	5.76E-10	4.27E-09	2.86E+04	2.14E+04	0.08	0.50	3.814E-06
60	9.61E-06	100	50	1.02E-05	424.5	0.076	3.069E+04	4.155E+05	3.70E-09	5.60E-12	3.74E-10	4.07E-09	2.79E+04	2.21E+04	0.05	0.51	3.416E-06
70	9.81E-06	400	50	1.04E-05	376.6	0.067	2.763E+04	1.836E+05	3.64E-09	5.49E-12	9.33E-10	4.57E-09	2.20E+04	2.80E+04	0.09	0.35	2.395E-06
70	9.81E-06	200	50	1.04E-05	355.0	0.063	2.605E+04	2.666E+05	3.64E-09	5.49E-12	5.48E-10	4.19E-09	2.26E+04	2.74E+04	0.06	0.39	2.311E-06
70	9.81E-06	100	50	1.04E-05	365.9	0.065	2.684E+04	3.765E+05	3.64E-09	5.49E-12	3.56E-10	4.00E-09	2.45E+04	2.55E+04	0.04	0.45	2.550E-06
80	1.00E-05	400	50	1.05E-05	408.2	0.073	3.038E+04	2.087E+05	3.59E-09	5.38E-12	8.89E-10	4.48E-09	2.43E+04	2.57E+04	0.10	0.39	2.834E-06
80	1.00E-05	200	50	1.05E-05	395.4	0.070	2.943E+04	3.115E+05	3.59E-09	5.38E-12	5.22E-10	4.11E-09	2.57E+04	2.43E+04	0.07	0.45	2.897E-06
80	1.00E-05	100	50	1.05E-05	420.3	0.075	3.128E+04	4.538E+05	3.59E-09	5.38E-12	3.39E-10	3.93E-09	2.86E+04	2.14E+04	0.05	0.52	3.495E-06
															0.07	**0.44**	
40	9.21E-06	400	100	9.92E-06	473.3	0.084	3.317E+04	1.977E+05	3.81E-09	5.84E-12	1.09E-09	4.90E-09	2.58E+04	7.42E+04	0.06	0.20	1.136E-06
40	9.21E-06	200	100	9.92E-06	442.9	0.079	3.104E+04	2.849E+05	3.81E-09	5.84E-12	6.40E-10	4.45E-09	2.66E+04	7.34E+04	0.04	0.23	1.074E-06
40	9.21E-06	100	100	9.92E-06	411.1	0.073	2.881E+04	3.625E+05	3.81E-09	5.84E-12	4.15E-10	4.23E-09	2.60E+04	7.40E+04	0.03	0.23	9.892E-07
60	9.61E-06	400	100	1.02E-05	943.6	0.168	6.821E+04	4.375E+05	3.70E-09	5.60E-12	9.81E-10	4.68E-09	5.39E+04	4.61E+04	0.11	0.43	3.646E-06
60	9.61E-06	200	100	1.02E-05	849.4	0.151	6.140E+04	6.066E+05	3.70E-09	5.60E-12	5.76E-10	4.27E-09	5.31E+04	4.69E+04	0.07	0.46	3.227E-06
60	9.61E-06	100	100	1.02E-05	813.6	0.145	5.881E+04	7.962E+05	3.70E-09	5.60E-12	3.74E-10	4.07E-09	5.34E+04	4.66E+04	0.05	0.48	3.110E-06
70	9.81E-06	400	100	1.04E-05	1538.5	0.274	1.129E+05	7.499E+05	3.64E-09	5.49E-12	9.33E-10	4.57E-09	8.99E+04	1.01E+04	0.18	0.72	2.701E-05
70	9.81E-06	200	100	1.04E-05	1411.8	0.251	1.036E-05	1.060E+06	3.64E-09	5.49E-12	5.48E-10	4.19E-09	9.00E+04	9.98E+03	0.12	0.78	2.520E-05
70	9.81E-06	100	100	1.04E-05	1363.6	0.243	1.000E-05	1.403E+06	3.64E-09	5.49E-12	3.56E-10	4.00E-09	9.11E+04	8.86E+03	0.08	0.83	2.741E-05
80	1.00E-05	400	100	1.05E-05	949.5	0.169	7.067E+04	4.855E+05	3.59E-09	5.38E-12	8.89E-10	4.48E-09	5.66E+04	4.34E+04	0.11	0.45	3.900E-06
80	1.00E-05	200	100	1.05E-05	896.1	0.160	6.670E+04	7.060E+05	3.59E-09	5.38E-12	5.22E-10	4.11E-09	5.82E+04	4.18E+04	0.07	0.51	3.820E-06
80	1.00E-05	100	100	1.05E-05	889.4	0.158	6.619E+04	9.602E+05	3.59E-09	5.38E-12	3.39E-10	3.93E-09	6.05E+04	3.95E+04	0.05	0.55	4.008E-06
															0.08	**0.49**	

Table B 2: Experimental results for single permeation experiments of CO_2

T (°C)	η (Pa.s)	P (kPa)	ΔP (kPa)	D_{Kn} $m^2.s$	ϕ_v ml/min	J mol/m^2.s	Knudsen ΔP (Pa)	Viscous ΔP (Pa)	D_{Kn}/RT mol/m2.s	(ε/τ)*r2/(8*η) $m^3/m^2.s$	mol/m^2.s	C tot	Support ΔP (Pa)	Membrane ΔP (Pa)	Vis %	Kn %	Permeability mol/m^2.s.Pa
40	1.57E-05	400	50	2.13E-06	115.8	0.0206	3.789E+04	8.236E+04	8.17E-10	3.43E-12	6.39E-10	1.46E-09	2.13E+04	2.87E+04	0.19	0.24	7.176E-07
40	1.57E-05	200	50	2.13E-06	102.7	0.0183	3.358E+04	1.124E+05	8.17E-10	3.43E-12	3.76E-10	1.19E-09	2.30E+04	2.70E+04	0.14	0.32	6.770E-07
40	1.57E-05	100	50	2.13E-06	118.0	0.0210	3.859E+04	1.771E+05	8.17E-10	3.43E-12	2.44E-10	1.06E-09	2.97E+04	2.03E+04	0.14	0.46	1.036E-06
60	1.66E-05	400	50	2.19E-06	106.8	0.0190	3.605E+04	8.566E+04	7.92E-10	3.24E-12	5.67E-10	1.36E-09	2.10E+04	2.90E+04	0.18	0.24	6.562E-07
60	1.66E-05	200	50	2.19E-06	105.3	0.0188	3.552E+04	1.300E+05	7.92E-10	3.24E-12	3.33E-10	1.13E-09	2.50E+04	2.50E+04	0.15	0.35	7.500E-07
60	1.66E-05	100	50	2.19E-06	111.9	0.0199	3.774E+04	1.894E+05	7.92E-10	3.24E-12	2.16E-10	1.01E-09	2.96E+04	2.04E+04	0.13	0.47	9.788E-07
70	1.71E-05	400	50	2.23E-06	89.8	0.0160	3.075E+04	7.618E+04	7.80E-10	3.15E-12	5.36E-10	1.32E-09	1.82E+04	3.18E+04	0.15	0.22	5.035E-07
70	1.71E-05	200	50	2.23E-06	107.9	0.0192	3.695E+04	1.410E+05	7.80E-10	3.15E-12	3.15E-10	1.10E-09	2.63E+04	2.37E+04	0.15	0.38	8.117E-07
70	1.71E-05	100	50	2.23E-06	102.7	0.0183	3.518E+04	1.840E+05	7.80E-10	3.15E-12	2.04E-10	9.85E-10	2.79E+04	2.21E+04	0.12	0.44	8.270E-07
80	1.75E-05	400	50	2.26E-06	104.4	0.0186	3.627E+04	9.360E+04	7.69E-10	3.07E-12	5.07E-10	1.28E-09	2.19E+04	2.81E+04	0.17	0.26	6.607E-07
80	1.75E-05	200	50	2.26E-06	94.9	0.0169	3.297E+04	1.311E+05	7.69E-10	3.07E-12	2.98E-10	1.07E-09	2.38E+04	2.62E+04	0.13	0.34	6.442E-07
80	1.75E-05	100	50	2.26E-06	85.2	0.0152	2.961E+04	1.613E+05	7.69E-10	3.07E-12	1.93E-10	9.63E-10	2.37E+04	2.63E+04	0.10	0.38	5.762E-07
															0.14	**0.34**	
40	1.57E-05	400	100	2.13E-06	209.2	0.0395	7.248E+04	1.576E+05	8.17E-10	3.43E-12	6.39E-10	1.46E-09	4.07E+04	5.93E+04	0.18	0.23	6.650E-07
40	1.57E-05	200	100	2.13E-06	187.6	0.0354	6.500E+04	2.177E+05	8.17E-10	3.43E-12	3.76E-10	1.19E-09	4.45E+04	5.55E+04	0.14	0.30	6.379E-07
40	1.57E-05	100	100	2.13E-06	182.9	0.0345	6.338E+04	2.909E+05	8.17E-10	3.43E-12	2.44E-10	1.06E-09	4.88E+04	5.12E+04	0.11	0.38	6.741E-07
60	1.66E-05	400	100	2.19E-06	233.6	0.0416	7.881E+04	1.873E+05	7.92E-10	3.24E-12	5.67E-10	1.36E-09	4.59E+04	5.41E+04	0.19	0.27	7.694E-07
60	1.66E-05	200	100	2.19E-06	211.0	0.0376	7.117E+04	2.606E+05	7.92E-10	3.24E-12	3.33E-10	1.13E-09	5.01E+04	4.99E+04	0.15	0.35	7.529E-07
60	1.66E-05	100	100	2.19E-06	204.2	0.0364	6.889E+04	3.456E+05	7.92E-10	3.24E-12	2.16E-10	1.01E-09	5.41E+04	4.59E+04	0.12	0.43	7.925E-07
70	1.71E-05	400	100	2.23E-06	235.0	0.0419	8.046E+04	1.993E+05	7.80E-10	3.15E-12	5.36E-10	1.32E-09	4.77E+04	5.23E+04	0.19	0.28	8.002E-07
70	1.71E-05	200	100	2.23E-06	220.6	0.0393	7.553E+04	2.882E+05	7.80E-10	3.15E-12	3.15E-10	1.10E-09	5.38E+04	4.62E+04	0.15	0.38	8.505E-07
70	1.71E-05	100	100	2.23E-06	206.2	0.0367	7.060E+04	3.692E+05	7.80E-10	3.15E-12	2.04E-10	9.85E-10	5.59E+04	4.41E+04	0.12	0.44	8.335E-07
80	1.75E-05	400	100	2.26E-06	216.5	0.03856	7.521E+04	1.941E+05	7.69E-10	3.07E-12	5.07E-10	1.28E-09	4.53E+04	5.47E+04	0.18	0.27	7.052E-07
80	1.75E-05	200	100	2.26E-06	192.3	0.03424	6.678E+04	2.655E+05	7.69E-10	3.07E-12	2.98E-10	1.07E-09	4.81E+04	5.19E+04	0.13	0.35	6.601E-07
80	1.75E-05	100	100	2.26E-06	192.1	0.03422	6.674E+04	3.636E+05	7.69E-10	3.07E-12	1.93E-10	9.63E-10	5.33E+04	4.67E+04	0.11	0.43	7.332E-07
															0.15	**0.34**	

Table B 3: Experimental results for single permeation experiments of CO

T (°C)	η (Pa.s)	P (kPa)	Δ P (kPa)	D_{Kn} $m^2.s$	ϕ_v ml/min	J $mol/m^2.s$	Knudsen ΔP (Pa)	Viscous ΔP (Pa)	D_{Kn}/RT mol/m2.s	$(\varepsilon/\tau)*r2/(8*\eta)$ $m^3/m^2.s$	$mol/m^2.s$	C tot	Support ΔP (Pa)	Membrane ΔP (Pa)	Vis %	Kn %	Permeability $mol/m^2.s.Pa$
40	1.84E-05	400	50	2.67E-06	144.4	0.0257	3.769E+04	1.202E+05	1.02E-09	2.93E-12	5.46E-10	1.57E-09	2.46E+04	2.54E+04	0.17	0.32	1.012E-06
40	1.84E-05	200	50	2.67E-06	138.7	0.0247	3.620E+04	1.779E+05	1.02E-09	2.93E-12	3.21E-10	1.34E-09	2.76E+04	2.24E+04	0.13	0.42	1.101E-06
40	1.84E-05	100	50	2.67E-06	138.8	0.0247	3.621E+04	2.439E+05	1.02E-09	2.93E-12	2.08E-10	1.23E-09	3.01E+04	1.99E+04	0.10	0.50	1.241E-06
60	1.93E-05	400	50	2.75E-06	167.4	0.0298	4.506E+04	1.555E+05	9.93E-10	2.80E-12	4.90E-10	1.48E-09	3.02E+04	1.98E+04	0.20	0.40	1.505E-06
60	1.93E-05	200	50	2.75E-06	147.6	0.0263	3.973E+04	2.112E+05	9.93E-10	2.80E-12	2.88E-10	1.28E-09	3.08E+04	1.92E+04	0.14	0.48	1.370E-06
60	1.93E-05	100	50	2.75E-06	152.1	0.0271	4.092E+04	2.981E+05	9.93E-10	2.80E-12	1.87E-10	1.18E-09	3.44E+04	1.56E+04	0.11	0.58	1.741E-06
70	1.96E-05	400	50	2.79E-06	128.0	0.0228	3.497E+04	1.247E+05	9.78E-10	2.75E-12	4.67E-10	1.44E-09	2.37E+04	2.63E+04	0.15	0.32	8.660E-07
70	1.96E-05	200	50	2.79E-06	125.5	0.0224	3.428E+04	1.883E+05	9.78E-10	2.75E-12	2.74E-10	1.25E-09	2.68E+04	2.32E+04	0.12	0.42	9.626E-07
70	1.96E-05	100	50	2.79E-06	120.0	0.0214	3.278E+04	2.467E+05	9.78E-10	2.75E-12	1.78E-10	1.16E-09	2.77E+04	2.23E+04	0.09	0.47	9.596E-07
80	2.01E-05	400	50	2.83E-06	99.4	0.0177	2.755E+04	1.023E+05	9.64E-10	2.68E-12	4.42E-10	1.41E-09	1.89E+04	3.11E+04	0.12	0.26	5.692E-07
80	2.01E-05	200	50	2.83E-06	99.4	0.0177	2.755E+04	1.575E+05	9.64E-10	2.68E-12	2.60E-10	1.22E-09	2.17E+04	2.83E+04	0.09	0.34	6.258E-07
80	2.01E-05	100	50	2.83E-06	97.8	0.0174	2.710E+04	2.123E+05	9.64E-10	2.68E-12	1.69E-10	1.13E-09	2.31E+04	2.69E+04	0.07	0.39	6.466E-07
															0.12	**0.41**	
40	1.84E-05	400	100	2.67E-06	284.3	0.0506	7.417E+04	2.366E+05	1.02E-09	2.93E-12	5.46E-10	1.57E-09	4.84E+04	5.16E+04	0.17	0.32	9.805E-07
40	1.84E-05	200	100	2.67E-06	254.6	0.0453	6.643E+04	3.265E+05	1.02E-09	2.93E-12	3.21E-10	1.34E-09	5.06E+04	4.94E+04	0.12	0.39	9.175E-07
40	1.84E-05	100	100	2.67E-06	240.9	0.0429	6.285E+04	4.234E+05	1.02E-09	2.93E-12	2.08E-10	1.23E-09	5.22E+04	4.78E+04	0.09	0.43	8.980E-07
60	1.93E-05	400	100	2.75E-06	306.8	0.0546	8.256E+04	2.849E+05	9.93E-10	2.80E-12	4.90E-10	1.48E-09	5.53E+04	4.47E+04	0.18	0.37	1.222E-06
60	1.93E-05	200	100	2.75E-06	271.6	0.0484	7.310E+04	3.886E+05	9.93E-10	2.80E-12	2.88E-10	1.28E-09	5.67E+04	4.33E+04	0.13	0.44	1.116E-06
60	1.93E-05	100	100	2.75E-06	258.5	0.0460	6.958E+04	5.068E+05	9.93E-10	2.80E-12	1.87E-10	1.18E-09	5.86E+04	4.14E+04	0.09	0.49	1.111E-06
70	1.96E-05	400	100	2.79E-06	245.9	0.0438	6.717E+04	2.395E+05	9.78E-10	2.75E-12	4.67E-10	1.44E-09	4.55E+04	5.45E+04	0.15	0.31	8.031E-07
70	1.96E-05	200	100	2.79E-06	220.9	0.0393	6.033E+04	3.314E+05	9.78E-10	2.75E-12	2.74E-10	1.25E-09	4.71E+04	5.29E+04	0.10	0.37	7.438E-07
70	1.96E-05	100	100	2.79E-06	222.5	0.0396	6.077E+04	4.575E+05	9.78E-10	2.75E-12	1.78E-10	1.16E-09	5.14E+04	4.86E+04	0.08	0.43	8.156E-07
80	2.01E-05	400	100	2.83E-06	201.6	0.0359	5.585E+04	2.073E+05	9.64E-10	2.68E-12	4.42E-10	1.41E-09	3.83E+04	6.17E+04	0.12	0.26	5.818E-07
80	2.01E-05	200	100	2.83E-06	186.6	0.03324	5.172E+04	2.957E+05	9.64E-10	2.68E-12	2.60E-10	1.22E-09	4.07E+04	5.93E+04	0.09	0.32	5.609E-07
80	2.01E-05	100	100	2.83E-06	183.6	0.0327	5.088E+04	3.986E+05	9.64E-10	2.68E-12	1.69E-10	1.13E-09	4.33E+04	5.67E+04	0.06	0.37	5.767E-07
															0.12	**0.37**	

Table B 4: Experimental results for the binary permeation CO and CO_2

Feed							Permeate											
Height		Area					Height		Area									
CO	CO2	CO	CO2	ΔP (kPa)	P (kPa)	Fraction CO	CO	CO2	CO	CO2	Permeate (ml/min)	Retentate (ml/min)	CO (ml/min)	CO2 (ml/min)	αCO/CO_2	Π_{CO}	Π_{CO2}	J_{CO}	J_{CO2}
3119	2862	21111	101787	100	100	0.8	3094	2832	22032	98766	156.0	154.2	123.3	30.7	1.00	5.72E-07	5.36E-07	2.20E-02	5.47E-03
3138	2877	21228	100317	100	200	0.8	3186	2922	22252	103224	168.5	145.0	137.2	34.2	1.00	6.36E-07	5.98E-07	2.44E-02	6.10E-03
3138	2893	21465	101746	100	400	0.8	3184	2909	22118	103356	183.5	125.0	149.2	37.1	1.01	6.92E-07	6.48E-07	2.66E-02	6.61E-03
Height		Area					Height		Area									
CO	CO2	CO	CO2	ΔP (kPa)	P (kPa)	Fraction CO	CO	CO2	CO	CO2	Permeate (ml/min)	Retentate (ml/min)	CO (ml/min)	CO2 (ml/min)	αCO/CO_2	Π_{CO}	Π_{CO2}	J_{CO}	J_{CO2}
7023	1290	86594	25896	100	100	0.2	7130	1264	89992	26143	178.4	140.9	36.2	140.1	1.03	6.71E-07	6.12E-07	6.44E-03	2.50E-02
7062	1287	88018	24685	100	200	0.2	7087	1279	89180	25725	188.7	121.7	38.0	150.0	1.01	7.05E-07	6.55E-07	6.77E-03	2.67E-02
7024	1285	87747	26248	100	400	0.2	7094	1300	88765	25909	207.9	106.4	41.9	167.9	1.00	7.78E-07	7.33E-07	7.46E-03	2.99E-02
Height		Area					Height		Area									
CO	CO2	CO	CO2	ΔP (kPa)	P (kPa)	Fraction CO	CO	CO2	CO	CO2	Permeate (ml/min)	Retentate (ml/min)	CO (ml/min)	CO2 (ml/min)	αCO/CO_2	Π_{CO}	Π_{CO2}	J_{CO}	J_{CO2}
5369	2207	54477	63391	100	100	0.5	5418	2181	55591	62852	170.9	152.2	86.5	85.0	1.02	6.42E-07	5.94E-07	1.54E-02	1.51E-02
5346	2183	54118	63434	100	200	0.5	5378	2179	54455	63155	183.5	132.8	92.2	91.2	1.01	6.84E-07	6.37E-07	1.64E-02	1.62E-02
5339	2188	54265	64133	100	400	0.5	5385	2191	55288	63369	200.9	115.6	101.1	100.4	1.01	7.50E-07	7.01E-07	1.80E-02	1.79E-02
Height		Area					Height		Area									
CO	CO2	CO	CO2	ΔP (kPa)	P (kPa)	Fraction CO	CO	CO2	CO	CO2	Permeate (ml/min)	Retentate (ml/min)	CO (ml/min)	CO2 (ml/min)	αCO/CO_2	Π_{CO}	Π_{CO2}	J_{CO}	J_{CO2}
5285	2136	53561	61722	100	100	0.5	5396	2166	55023	61769	171.8	327.9	88.8	87.4	1.02	6.59E-07	6.10E-07	1.58E-02	1.56E-02
5195	2121	52653	60152	100	200	0.5	5344	2138	54946	61046	189.1	320.0	96.8	94.9	1.02	7.18E-07	6.63E-07	1.72E-02	1.69E-02
5177	2130	52090	61256	100	400	0.5	5291	2150	54119	60942	204.3	296.5	103.5	103.1	1.00	7.68E-07	7.20E-07	1.84E-02	1.84E-02

Table B 5: Experimental results for the binary permeation H_2 and CO

Feed							Permeate											
Height		Area					Height		Area									
CO	H2	CO	H2	ΔP (kPa)	P (kPa)	Fraction CO	CO	H_2	CO	H_2	Permeate (ml/min)	Retentate (ml/min)	CO (ml/min)	H_2 (ml/min)	$\alpha H_2/CO$	Π_{CO}	Π_{H2}	J_{CO}	J_{H2}
6764	111	84959	453	100	100	0.8	6775	117	84292	450	178.8	141.2	142.8	37.8	0.94	6.624E-07	6.603E-07	2.54E-02	6.73E-03
6762	110	84734	458	100	200	0.8	6831	108	85642	358	209.4	106.1	168.6	40.7	1.04	7.821E-07	7.104E-07	3.00E-02	7.25E-03
6834	111	86768	381	100	400	0.8	6883	95	86840	298	220.6	94.5	179.0	37.9	1.18	8.301E-07	6.613E-07	3.19E-02	6.75E-03
Height		Area					Height		Area									
CO	H2	CO	H2	ΔP (kPa)	P (kPa)	Fraction CO	CO	H_2	CO	H_2	Permeate (ml/min)	Retentate (ml/min)	CO (ml/min)	H_2 (ml/min)	$\alpha H_2/CO$	Π_{CO}	Π_{H2}	J_{CO}	J_{H2}
2859	228	21338	1141	100	100	0.2	2780	220	20552	1389	324.3	35.7	63.6	252.2	1.01	1.180E-06	1.101E-06	1.13E-02	4.49E-02
2872	225	20956	1154	100	200	0.2	2511	241	17488	1626	295.6	58.1	52.4	251.8	0.83	9.714E-07	1.099E-06	9.33E-03	4.48E-02
2774	226	20590	1160	100	400	0.2	2611	235	18718	1415	241.9	115.6	44.6	200.7	0.89	8.271E-07	8.760E-07	7.94E-03	3.57E-02
Height		Area					Height		Area									
CO	H2	CO	H2	ΔP (kPa)	P (kPa)	Fraction CO	CO	H_2	CO	H_2	Permeate (ml/min)	Retentate (ml/min)	CO (ml/min)	H_2 (ml/min)	$\alpha H_2/CO$	Π_{CO}	Π_{H2}	J_{CO}	J_{H2}
5344	184	55995	807	100	100	0.5	5264	190	54617	925	283.0	31.1	139.1	147.4	0.94	1.032E-06	1.030E-06	2.48E-02	2.63E-02
5359	176	55919	646	100	200	0.5	5267	186	54243	915	284.4	41.9	139.9	145.4	0.96	1.038E-06	1.015E-06	2.49E-02	2.59E-02
5359	186	56218	849	100	400	0.5	5324	184	55931	961	297.0	27.4	140.7	142.8	0.99	1.044E-06	9.971E-07	2.51E-02	2.54E-02
Height		Area					Height		Area									
CO	H2	CO	H2	ΔP (kPa)	P (kPa)	Fraction CO	CO	H_2	CO	H_2	Permeate (ml/min)	Retentate (ml/min)	CO (ml/min)	H_2 (ml/min)	$\alpha H_2/CO$	Π_{CO}	Π_{H2}	J_{CO}	J_{H2}
5008	180	52057	763	100	100	0.5	4690	197	46879	794	283.7	208.3	130.1	153.6	0.85	9.655E-07	1.072E-06	2.32E-02	2.73E-02
5160	185	53188	744	100	200	0.5	4785	195	48248	806	297.0	203.8	139.0	159.1	0.87	1.031E-06	1.112E-06	2.48E-02	2.83E-02
5174	181	54751	746	100	400	0.5	5073	190	52259	841	297.0	200.9	147.4	155.1	0.95	1.094E-06	1.083E-06	2.62E-02	2.76E-02

Table B 6: Experimental results for the binary permeation H_2 and CO_2

Feed							Permeate											
Height		Area					Height		Area									
CO	H2	CO	H2	ΔP (kPa)	P (kPa)	Fraction H_2	H_2	CO_2	H_2	CO_2	Permeate (ml/min)	Retentate (ml/min)	H_2 (ml/min)	CO_2 (ml/min)	$\alpha H_2/CO_2$	Π_{H2}	Π_{CO2}	J_{H2}	J_{CO2}
2222	175	65102	880	100	100	0.5	2131	198	61070	944	242.1	77.9	116.9	135.6	0.86	8.68E-07	9.47E-07	2.08E-02	2.42E-02
2214	177	65092	1022	100	200	0.5	2147	184	58652	919	237.6	82.4	115.6	124.0	0.93	8.58E-07	8.66E-07	2.06E-02	2.21E-02
2185	177	64012	925	100	400	0.5	2164	179	62979	897	235.1	84.9	115.2	119.3	0.97	8.55E-07	8.33E-07	2.05E-02	2.12E-02

APPENDIX C: EXPERIMENTAL PROCEDURES

CHARACTERISATION

For characterisation experiments the following procedure was followed:

1. Position 1 *(Refer to Figure 3-2)* is blanked off while feed enters the membrane through position 2 directly from the gas regulator. A pressure gauge (Control Instruments 0-600 kPa) is attached to position 3 and a soap flow meter is connected at position 4.
2. Gas flow (SF_6, H_2, CO_2, CO and N_2) is introduced into the membrane until the gauge reads 1 bar.
3. After steady state (usually not more than 2 minutes) is reached, readings are taken on the soap flow meter.
4. This can be repeated at different feed pressures as required.

PERMEATION EXPERIMENTS

Permeation experiments were more complicated and involved more variables with temperature and feed pressure being the most important. The procedure for binary and ternary experiments was as follow:

1. With the membrane firmly in the module, the module is placed inside the oven.
2. The mass flow controller's (MFC) for the desired situation (depending on the type of experiment, composition of mixture etcetera.) were set to the desired flow rate using the appropriate calibration curve *(see appendix A: MFC calibration)*.

The following steps are done to determine the response factor, which together with the total permeate flow rate, is used to determine the actual component flow *(See equation 3-1)*.

$$k = \frac{C_F}{A_F} \text{ or } k = \frac{C_F}{A_F} \qquad \text{C.1}$$

with C_F the feed concentration,

A_F the area counts determined by a chromatogram of the feed, and

H_F the height counts determined by a chromatogram of the feed.

3. Set the 3-way valves as to follow loops A1 and B2 with valves 1, 3 and 4 closed and valve 2 open.
4. Allow the flow to stabilise (2-3 minutes).
5. Switch to loop B1 and open valves 3 and 4 immediately for approximately 10 seconds.
6. Press RUN on the GC and close valves 3 and 4 after the GC's pneumatic sampling valve switches position.
7. Keep loop B1 active and wait for the GC to finish its run.
8. After the sampling valve switches to its original position, change back to loop B2.

The following steps are done to determine the concentration of the actual component flow *(See equation 3-2).*

$$C_{Perm} = k.A_{Perm} \text{ or } C_{Perm} = k.H_{Perm} \qquad \text{C.2}$$

with C_{Perm} the permeate concentration,

A_{Perm} the area counts determined by a chromatogram of the permeate, and

H_{Perm} the height counts determined by a chromatogram of the permeate.

9. Set the 3-way valves as to follow loops A2 and B2 with valves 1, 3 and 4 closed and valve 2 open.
10. Set the backpressure regulators to give the required feed pressure and trans membrane pressure.

11. Allow the flow to stabilise (5 minutes).
12. Repeat steps 5 to 8.
13. To determine the permeate flow rate keep loop A2 active and close valve 2.
14. Open valve 1 and take measurements from the soap flow meter.

For single gas experiments the GC were not used. The procedure was as follow:

1. Repeat steps 1 to 2.
2. Set the 3-way valve to follow loop A2.
3. Close valve 2 and open valve 1.
4. Take soap flow meter measurements.